February 2015

Gravity, Magnetic, and Geologic Constraints on the Raton Basin of Southern Colorado, USA

Yusuf Pehlivan
Florida State University

FLORIDA STATE UNIVERSITY

COLLEGE OF ARTS AND SCIENCES

GRAVITY, MAGNETIC, AND GEOLOGIC CONSTRAINTS ON THE RATON BASIN OF SOUTHERN COLORADO, USA

By

YUSUF PEHLIVAN

A Thesis submitted to the
Department of Earth, Ocean, and Atmospheric Sciences
in partial fulfillment of the
requirements for the degree of
Master of Science

Degree Awarded:
Spring Semester, 2015

Yusuf Pehlivan defended this thesis on February 4, 2015.

The members of supervisory committee were:

David Farris
Professor Directing Thesis

James F. Tull
Committee Member

Stephen Kish
Committee Member

The Graduate School has verified and approved the above-named committee members, and certified that the thesis has been approved in accordance with university requirements.

To my mother, my siblings, and my fiancé

ACKNOWLEDGMENTS

So many people were involved directly or indirectly in this study. I wouldn’t finish my thesis without their supports and encouragements. First and foremost, I express my sincerest gratefulness to my advisor Dr. David Farris, whose ceaseless efforts and patience helped me guide through this thesis. His comprehensive knowledge of the Raton Basin and his ambition toward field geology is admirable. I’ve learnt priceless knowledge both in the field and thesis preparation stages from him. I consider myself extremely lucky to have worked under his guidance.

I would also like to thank my committee members, Dr. Stephane Kish and Dr. James Tull, for being my committee members and sharing their experiences with me. Their support and feedbacks helped me in all the time of my study.

I would like to thank Turkish community in Tallahassee who share their graduate study experiences with me and support and encourage me any time during this study. I also would like to thank my friends for the inspiring conversations I have had with; my roommate Gokhan Tekin for his help, my classmate Ali Can Altintas for his encouragement and help, my Turkish friends, Umit Tokac, Ahmet Serhat Gozutok, Oktay Akpolat, Riza Memis and Dogan Guner for their support. I’ve learnt a lot from them.

I would like to send a special appreciation to the faculty members of the department of Geological Engineering at Dumlupinar University. In the first instance, I would like to thank Associated Professor Zeynal Abiddin Erguler and M. Serkan Akkiraz for their faith to me. They helped me as much as possible during my study. Professor Yasar Kibici, department chair, deserves heartfelt acknowledge for his encouragement and support.

I also would like to thank to the Turkish Petroleum Corporation for this scholarship and providing a great opportunity in U.S with full financial support.

Last but not least; I kept the greatest appreciation for my family members and my fiancé. I would like to thank my mom, my sisters and my brother who never lost their faith to me. Emine Cakir, my love, deserves so many thanks for her patient, support and eternal love during the last 2.5 years. It wouldn't have been possible to finish my thesis without her. As the end, I would like to send my pray and gratefulness to my dad. I know, he would have been proud of me if he had lived.

TABLE OF CONTENTS

LIST OF FIGURES

LIST OF TABLES

ABSTRACT

The overall goal of this project is to better understand geologic characteristics of the Raton Basin. The Raton Basin is a Rocky Mountain foreland basin that contains Pennsylvanian through modern sedimentary rocks. The current structure of the basin is thought to have formed during the late Cretaceous through Tertiary Laramide orogeny. During this event, the basin was folded into a syncline, and steep reverse faults formed along the western edge of the basin in which Pre-Cambrian crystalline rocks of the Sangre de Cristo Range were partially thrust over the basin itself. In the Oligocene through present, the tectonic environment of the basin has been dominated by extension and extensional magmatism related to the Rio Grande Rift. A series of small plutonic bodies and more spatially extensive magmatic dikes intruded into the basin over this time interval.

A high-resolution gravity transect with approximately 70 stations was conducted across the Raton Basin near the Spanish Peaks. This transect, coupled with existing data, indicate a 20 mgal negative Bouguer gravity anomaly in the northern part of the basin and a 55-60 mgal negative anomaly in the south. Gravity models of these observations indicate that the Raton Basin is approximately 3 km thick in the north and 5 km thick in the south. Also, the basin is structurally deformed into an asymmetric synform that is tightest in the central part of the basin.

High-resolution magnetic measurements were also taken to better understand the structure of the numerous dikes in the region. Magnetic susceptibility measurements were used to constrain induced magnetism of the igneous rocks. However, the total field strength of magnetic anomalies associated with the dikes indicates that normal and reversed polarity remnant magnetism is also significant.

CHAPTER 1

INTRODUCTION

1.1 Overview

The Raton Basin is a Laramide Rocky Mountains foreland basin but it distinctively has a complex structural and stratigraphical history. The basin has well-exposed sedimentary sequences ranging in age from Pennsylvanian up to current alluvial sediments (Cooper, 2006). Furthermore, the sedimentary rocks on the west limb of the basin dip steeply eastward and they are extensively deformed by thrust faults and folds. However, the sedimentary rocks on the east limb of the basin dip gently westward.

The Raton Basin extends from Southern Colfax County, New Mexico to Huerfano County, Colorado. It is 128 km long from north to south, and 80 km wide from west to east. The basin is constrained on the west by the Sangre de Cristo Mountains, on the east by Sierra Grande uplift. The northern limit is characterized by Wet Mountains and Apishapa arch, and the southern boundary is identified by Tucumcari Basin (Figure 1.1). However, the survey area includes just a part of the Raton Basin, near the Spanish Peaks, located in Southern Colorado.

In the Late Oligocene to Early Miocene the Raton Basin was extensively intruded by stocks, sills, and dikes. Many of them form mountains and hills, and dominate the landscape. Dikes are the remarkable example for radial dikes. The Spanish Peaks are the largest igneous masses in the basin, and they are classified as stocks.

Gravity and magnetic surveys in company with geologic observations have been performed to delineate the structural patterns of the basin. Quantitative models have been constituted using gravity and magnetic readings in the basin. These models will help to understand the geometry of the igneous rocks as regards the sedimentary rocks.

The goal of this thesis is to better understand geological characteristics of the Raton Basin by using geophysical techniques. In order to assess these relationships, structural patterns and geological features of the Raton Basin will be discussed.

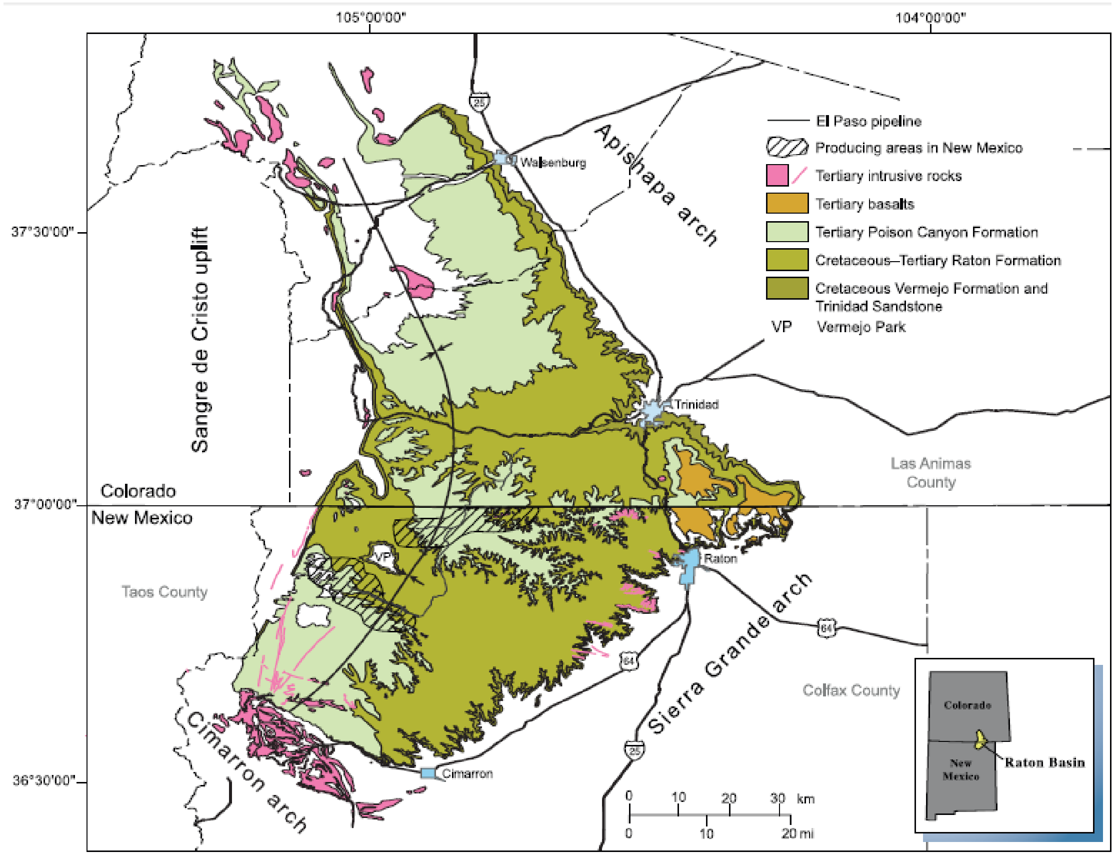

Figure 1.1. Generalized geologic map of the Raton Basin showing the location and geologic boundaries of the study area. Derived from New Mexico Bureau Geology and Mineral Resource (2003) and Tweto (1979) (Hoffman and Brister, 2003).

1.2 Geological Settings of the Raton Basin

1.2.1 Stratigraphic History of the Raton Basin

The Raton basin formed during the Laramide orogeny, and is the southernmost of several major coal-bearing basins along the eastern margin of the Rocky Mountains. It contains sedimentary rocks as old as Devonian overlying Proterozoic basement rocks with Quaternary sediments at the surface (Table 1.1). Additionally, major sedimentary units in the basin are

Eocene – Oligocene in age. The sedimentary sequence exposed within the Raton Basin was deposited in association with regression of the Cretaceous Interior Seaway (Cooper, 2006). During the early Paleozoic time, "Continental Backbone" covered the most of the area of the Raton Basin. Continental Backbone is a term that is characterized by very little sedimentation. Then, Ancestral Rocky Mountains began to rise about 320 million years ago during Pennsylvanian time (Lindsey, 2010). However, Ancestral Rocky Mountains were worn down by erosion by the end of the Permian time (Lindsey, 2010). Present Sangre de Cristo range uplifted, and sediments accumulated into the central Colorado. The Pennsylvanian Sangre de Cristo formation corresponds to sedimentary fill that was formed due to erosion occurred after the Sangre de Cristo uplift (Lindsey, 2010). The Sangre de Cristo formation is composed of fluvial arkosic sandstones and conglomerates.

The Yeso formation, Glorieta sandstone and Bernal formation were deposited as a result of the seas returned, and covered the Raton Basin region after the Early Permian orogeny (Speer, 1976). The Yeso formation consists of shale and fine grained sandstone. The Glorieta sandstone is composed of grey, fine to medium grain, well-sorted marine sandstones. The Bernal formation which is lithologically similar to the Yeso formation consists of siltstone, shale and fine to coarse grained sandstone.

The Dockum group and Johnson Gap formation were deposited as terrestrial rocks of the late Triassic age. They were laid down as a blanket of sandstone and shale over the Raton Basin. The Dockum group consists of red sandstone and shale. The rocks of the late Triassic age are referred to the Dockum group in most of the Raton Basin. The Johnson Gap formation is composed of siliceous limestone conglomerate, shale, and grey and red sandstone.

In late Jurassic time, a widespread blanket of shallow marine and overlying terrestrial deposits were laid down across the Raton Basin (Baltz, 1965). The Entrada sandstone and Morrison formation were deposited in Late Jurassic time. The Entrada sandstone is the basal upper Jurassic unit in almost the entire region. The Entrada composes of white to pink and red, fine to coarse grained sandstone fragments (Baltz, 1965). The Morrison formation consists of terrestrial sandstone and shale.

The Dakota sandstones are fine-grained and well-sorted as a result of a transgressing littoral environment (Speer, 1976). The Niobrara formation which is of marine origin overlies the Dakota sandstones. It consists of a basal limestone member and shale interbedded with thick, silty, calcareous mudstone. The marine Pierre shale conformably overlies the Niobrara formation. The Pierre shale intertongues with Trinidad sandstone. The upper part of the Pierre shale becomes sandy and forms a gradual transition zone. This transition zone marks the final regression of the Western Interior Seaway in the Raton basin.

The Western Interior Seaway controlled the depositional environment during the upper Cretaceous period. The Raton basin contains a nearly complete Cretaceous and Tertiary stratigraphic sequence of sedimentary rocks that include coal-bearing Vermejo and Raton formations (Close and Dutcher, 1990a) (Figure 1.2).

The upper Trinidad sandstone intertongues with and is overlain by the coal bearing Vermejo formation (Tremain, 1980). The Vermejo Formation consists of poorly sorted greywacke sands, gray, carbonaceous, silty shales, and thin- to thick-bedded, lenticular coal beds (Speer, 1976). Depositional environments of the sediments in the Vermejo formation include lagoonal, coastal swamp, and flood plain environments. It contains laterally extensive coal beds.

The Upper Cretaceous and Paleocene Raton formation lies unconformably above the Vermejo formation. Syndepositional clastic sediments shed off from the Sangre de Cristo Mountains, and they were deposited as the Raton basal conglomerate. The Raton basal conglomerate unit acts as a line which shows the erosional contact between the Raton formation and the Vermejo formation. The Raton formation also has a basal sandstone sequence that consists of fine-to-medium grained, fluvial sandstones. This basal unit is overlain by a coal-bearing shale sequence, a thick, coarse-grained sandstone sequence and another coal-bearing shale sequence, totaling as much as 2,000 ft of strata in some areas of the basin (Speer, 1976).

The Vermejo and Raton formations are two prominent coal-bearing units in the basin. However, the Raton formation contains more coal than the Vermejo formation. The underlying reason is that coal seams in the Vermejo formation are thinner and more discontinuous. The Vermejo formation was deposited in a lagoon environment whereas the Raton formation was deposited in a fluvial depositional environment. The Raton formation grades into the alluvial fan deposits of the Poison Canyon formation (Cooper, 2006).

Syn-Laramide orogenic sedimentation occurred during Tertiary time. The Sangre de Cristo uplift that began to rise in the Laramide orogeny supplied these synorogenic rocks (Woodward, 1976). Syn-Laramide deposition is recorded by the Paleocene Poison Canyon formation, Eocene Cuchara and Huerfano formations, and Oligocene Farisita formation. The Poison Canyon Formation consists of coarse, poorly-sorted, conglomeratic arkose; sandstones interbedded with thin yellow clay siltstones (Speer, 1976). The Poison Canyon formation is considered to have good petroleum potential due to the fact that the end of the deposition shows marine affinities. The Cuchara formation consists of red conglomeratic sandstones and thin variegated shale with abundant dikes and sills that are evidence of Rio Grande rift related magmatism. The Huerfano formation composes of variegated shale and conglomeratic sandstone. Postorogenic rocks and sediments were accumulated in the basin during late Tertiary to Quaternary time (Woodward, 1976).

Table 1.1. Stratigraphic Column for the Raton Basin. (Cooper, 2006).

	Geologic Age	Formation	Thickness in Feet	Lithology
	Quaternary	Recent	0-30	Alluvium and basalt flows
Tertiary	Miocene	Devils Hole and igneous activity	25-1300	Tuff and volcanic conglomerate, igneous intrusives throughout section
	Oligocene	Farisita	0-1200	Arkosic conglomerate
	Eocene	Huerfano	0-2000	Variegated shale and conglomeratic sandstone
		Cuchara	0-5000	Red conglomeratic sandstone with thin variegated shale
	Paleocene	Poison Canyon	0-2500	Arkosic sandstone and conglomerate with thin shale
Mesozoic	Late Cretaceous	Raton	0-1700	Thin coal beds, sandstone, shale and basal conglomerate
		Vermejo	0-550	Sandstone, shale and coal
		Trinidad Sandstone	0-300	Fine-grained beach sand
		Pierre Shale	1600-2300	Grey marine shale, sandy shale and sandstone
	Early Cretaceous	Niobrara	550-630	Marine shale and limestone
		Carlile Shale	155-235	Dark grey marine shale
		Greenhorn Limestone	35-80	Thin-bedded limestone
		Graneros Shale	185-385	Dark grey marine shale
		Dakota Sandstone	100-150	Grey massive sandstone
		Purgatoire	100-150	
	Jurassic	Morrison		Continental shale, sandstone
		Ralston, Todilto and Entrada	100-600	Marine sediments, gypsum and beach sandstone
	Triassic	Johnson Gap	0-700	Limestone conglomerates
		Dockum Group	0-1200	Red sandstone, calcareous shales and thin limestones
Paleozoic	Permian	Bernal	0-150	Continental Sediments
		Glorieta	0-200	Marine sandstones
		Yeso	0-250	Red silt, shale and sandstone
	Pennsylvanian	Sangre de Cristo	250-5400	Variegated shales, arkoes, conglomerates and thin marine limestones
	Precambrian	Precambrian	Basement	Mafic gneiss, quartzite, granite and granite gneiss

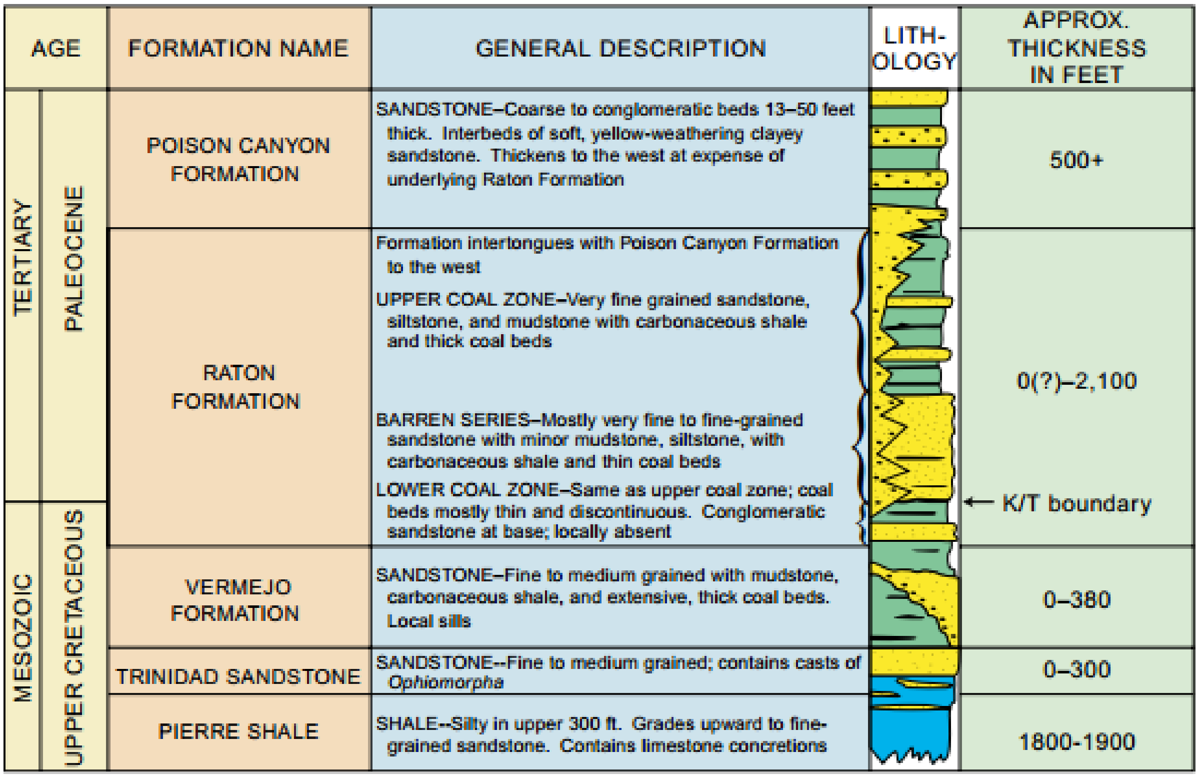

Figure 1.2. Generalized stratigraphic column of Cretaceous and Tertiary rocks in the Raton Basin part of the Raton Basin–Sierra Grande Uplift Province. Wavy gray line marks erosional unconformity between Vermejo and Raton Formations. (Cooper, 2006).

1.2.2 Basin Structure

The Laramide orogeny in the region began about 67.5 Ma and ended about 50 Ma (Tweto, 1975). The basin is characterized by a syncline. The La Veta syncline substantially plays an important role in the formation of the basin (Figure 1.3). The syncline axis roughly cuts in the middle of the basin. The Sangre de Cristo uplift occurred during the Laramide orogeny, as high angle limited over-thrusts of primarily sedimentary material were thrust up and over the Raton Basin (Woodward, 1987). Overturned sedimentary strata appear at the western edge of the basin. The La Veta syncline represents the axial trace of the basin. The Greenhorn Anticline and Del Carbon Syncline that are located in the northern portion of the Raton Basin show increase the strength of structural complexity (Figure 1.5). It lies parallel to the Sangre de Cristo Mountains.

The western flank of the basin dips steeply and has been affected by substantial thrust faults. Sedimentary rocks along the western edge of the basin are extensively deformed by steep dipping thrust faults and several major folds (Hemborg, 1998). However, the eastern flank of the basin dips gently to the west. Generalized geologic cross section through the Southern Raton Basin is given in Figure 1.4 to demonstrate the general shape of the basin.

Igneous activity has occurred within and adjacent to the basin since Miocene times with ages ranging from approximately 26 to 21 million years until present (Penn, 1995; Miggins, 2002; Lee, 2005). This igneous activity mostly occurred as intrusions such as stocks, laccoliths, dikes and sills (Figure 1.6). Igneous rocks types are various in the basin such as granites, syenites, diorites and gabbros (Johnson, 1968). All types of igneous rocks in the basin dominate the topography. However, various types of dikes and sills shape the current basin topography.

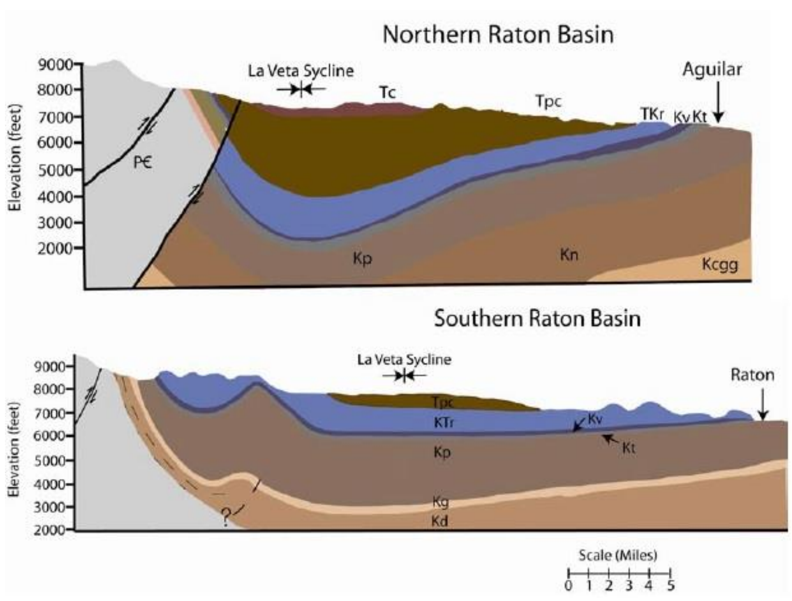

Figure 1.3. Structural cross sections perpendicular to the basin axis for both the northern and southern portions of the basin. 1/1000 vertical exaggeration (Cooper, 2006).

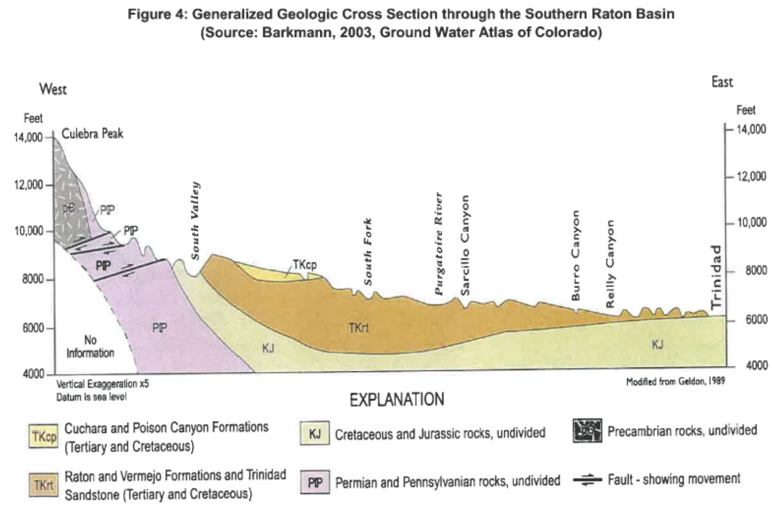

Figure 1.4. Generalized geologic cross section through the Southern Raton Basin (taken from the paper named by Freeman 3-24 well Nontributary determination Huerfano County, Colorado Raton Basin prepared by AMEC Environmental & Infrastructure, INC., 2012).

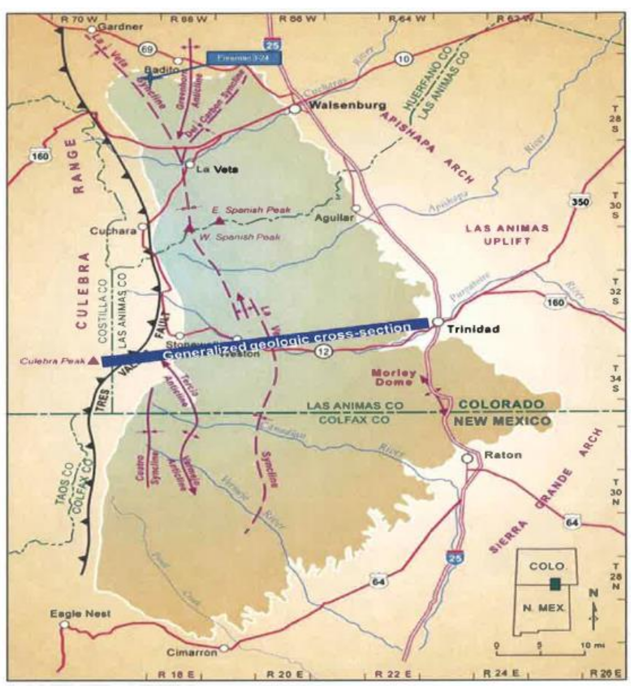

Figure 1.5. Structural map of the Raton Basin (Source S.S. Papadopulos & Associates, Inc. in conjunction with CGS, 2007) (taken from the paper named by Freeman 3-24 well Nontributary determination Huerfano County, Colorado Raton Basin prepared by AMEC Environmental & Infrastructure, INC., 2012).

The Spanish Peaks are the best known and prominent intrusions in the Raton Basin (Johnson, 1968). They are characterized by a radial dike swarm, and classified as stocks. Numerous sills and characteristic dikes are associated with the Spanish Peaks.

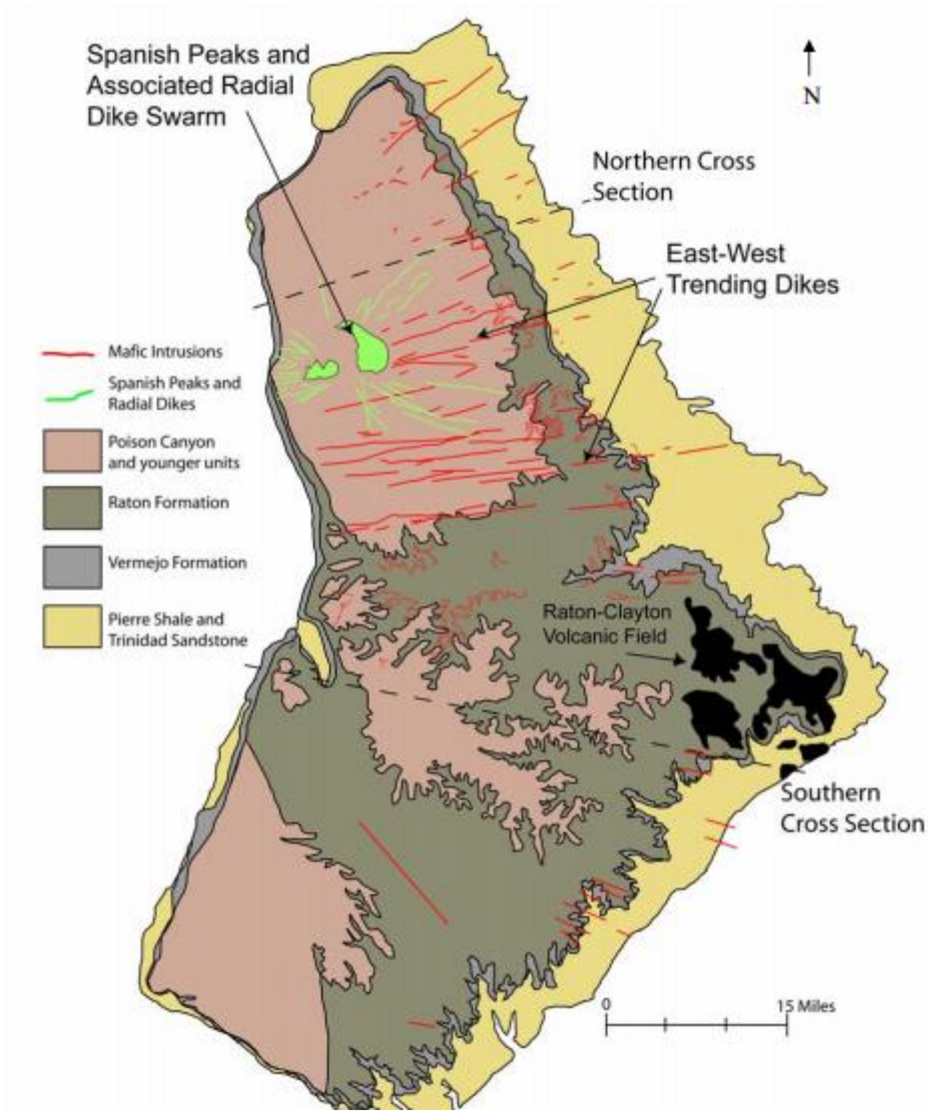

Figure 1.6. Raton Basin Intrusion map (Cooper, 2006).

1.3 Petrography of Igneous Rocks

In the Raton Basin most igneous rocks were emplaced during late Oligocene to early Miocene time and intruded the sedimentary rocks of the basin. The igneous bodies do not exhibit significant structural deformation because they were emplaced after the Raton basin had been structurally developed and the Laramide thrusting of the Sangre de Cristo Mountains had subsided (Figure 1.7).

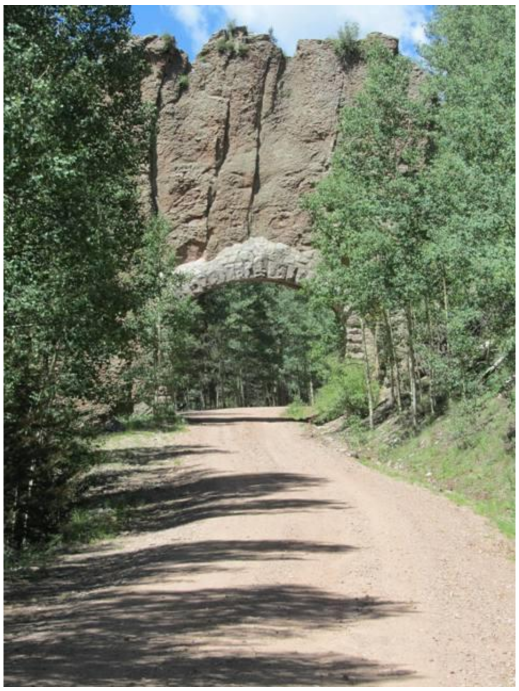

Figure 1.7. Dike with archway cut through it for road. Location is southwest of West Spanish Peak. View is westward.

The igneous rocks in the Raton basin region construct a continuous transition from granite to gabbro. These rocks are chemically in range from acidic to ultrabasic and from oversaturated to undersaturated types. They are also mafic to felsic (Johnson, 1968).

The sequence of intrusions in the Raton Basin generally seems to form silicic to mafic. Therefore, the oldest intrusive is the East Spanish Peak and mafic dikes and sills are the youngest intrusive features in the region. Late Oligocene to Early Miocene age intrusive features around the Spanish Peaks cause contact metamorphic rocks to form (Johnson, 1968). Bleached sandstone and baked shale are locally seen around the Spanish Peaks where dikes and sills come up. However, next to the largest intrusive bodies, contact metamorphism is very prominent. Conglomerate, sandstone, and shale beds have been altered to conglomeratic quartzite, hornfels, and slate (Johnson, 1961). Petrographically, the igneous rocks have variety which shows a continuous gradation from granite to gabbro. These include phaneritic, aphanitic, and porphyritic varieties of granite, granodiorite, syenite, syenodiorite, diorite, syenogabbro, and gabbro as well as lamphophyric varieties of syenite, syenodiorite, diorite, syenogabbro, and gabbro (Johnson, 1961) (Figure 1.8).

Figure 1.8. Porphyritic dike with a zone of plagioclase feldspar.

CHAPTER 2

FIELD WORK DESCRIPTION AND DATA COMPILATION

2.1 Introduction of Field Work for Gravity Survey

The purpose of the gravity survey is to reveal geologic and structural characteristics of the Raton Basin. In this study, a gravity survey was performed using a Worden gravimeter to better understand structural geometry of the Raton basin and the distribution of intrusive rocks. The survey consists of a transect perpendicular to the strike of the Raton basin composed of 77 measurements. Locations of stations are shown on figure 2.1. There is a high resolution segment across the main thrust and a lower resolution segment cross the West Spanish Peak and extends across the basin. Station elevations were measured by Trimble Pro XRT differential GPS receiver. (Figure 2.2) Elevation precision is mostly lower than ± 10 cm. EGM96 was used for the vertical datum.

Observed gravity is affected by tidal effects, elevation and instrument drift as a function of time at a given location. Corrections should be applied on gravity data to get rid of these effects.

In order for a gravity survey to be interpreted in terms of geology, so we must dismiss undesirable elevation effect, which is known as the “free-air” effect. Free-air effect has been taken into account during calculation of gravity anomalies. Gravimeters are very sensitive instruments and can drift gradually with time. Repeated readings at a same location are needed to address this issue to obtain accurate data. A base station was designated and readings at this location were taken twice in a day to account for instrument drift. Repeated measurements indicate precision of the gravity values is approximately ± 0.2 mGal. Based on tie-ins to previously measured stations, the accuracy of the absolute gravity measurements is ± 1 mGal.

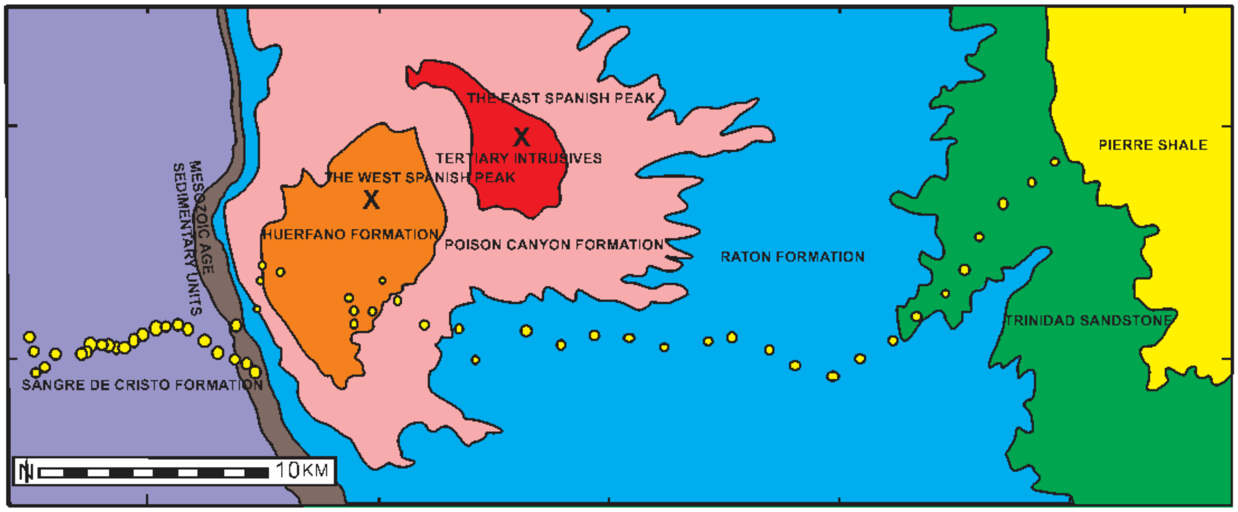

Figure 2.1. Geologic map of the Raton basin showing the location of gravity stations. Modified form the state geologic map.

Rock samples were collected for laboratory works. Rock densities and magnetic susceptibility were determined in the laboratory and used to constrain gravity and magnetic models. The way to measure the density of a rock sample is to weight the sample in the air and then submerged water. If ωa is the weight of the sample in air and ωw is its weight when immersed in water, then its density is:

$$\rho = \omega a / (\omega a - \omega w)$$

The water is assuming as pure H_2O at 25C°. Density table is shown in table 2.1 (Appendix A).

2.1.1. Free-Air Correction

The free-air correction accounts for gravity variations caused by elevation differences in the observation locations. Sea level is commonly considered as the reference level because gravity decreases 0.3086 mGal/m. This correction must be added for stations above sea level.

2.1.2. Simple Bouguer Gravity Correction

The Simple Bouguer correction accounts for excess mass underlying observation points where elevation of an observation point is higher than elevation of the datum. The Simple Bouguer correction provides to discard slab effect on the Bouguer anomaly. It is applied as a positive value added to the Bouguer anomaly.

Figure 2.2. Tools were used during our fieldwork. Trimble Pro XRT differential GPS receiver and Worden gravimeter.

Simple Bouguer anomaly is the anomaly caused by subsurface density contrast. It is calculated by extraction of calculated gravity form observed gravity. There are three main components such as latitude effect, free-air effect, and Bouguer effect for measuring calculated gravity. Formula of the calculated gravity is:

$$\delta_{calculated} : \delta_{lat} + \delta_{fe} + \delta_{bouguer}$$

Hence, the Simple Bouguer gravity anomaly is:

$$\delta_{BA\,:}\,\delta_{observed} - \delta_{calculated}$$

The average crustal density of 2.67 g/cm^3 was considered to compute the Bouguer correction. Using an average crustal density of 2.67 g/cm^3 is the common practice for calculating Bouguer gravity anomaly.

2.1.3. Bouguer Spherical Cap Correction

The Bouguer spherical cap models a simple mass from the ellipsoid to the station height. The density of the mass normally is the average continental density of 2.67 g/cm3 (Hinze, 2003). Bouguer slab correction was used in older methods for reducing gravity data. However, Bouguer slab correction is created depend on a flat Earth model (Holom and Oldow, 2007). The Bouguer spherical cap correction clarifies errors caused by the curvature of Earth (Hildebrand et al., 2002). Bouguer spherical cap correction was applied to the gravity data.

2.1.4. Terrain Correction

The terrain correction accounts for variation of topographic mass. The terrain correction is applied during a procedure of computing the gravity data. It is necessary and important in dealing with gravity data. Regardless of topography, mountain or valley, the terrain correction is positive. The terrain correction formula is given by:

$$\delta_t = \delta_{obs\,+}\,\delta_{lat} + 0.3086h - 0.04193rh + TC \text{ (mGal)}$$

TC is the value of the computed Terrain correction.

Terrain correction for this study is necessary due to the large elevation change. Elevation of the survey area is ranges from2000 to 3300 meters and this large change in altitude can significantly alter observed gravity anomalies. Therefore, the first thing to do before interpretation of the new gravity data is amendment on Bouguer anomaly using interpolated terrain correction. Interpolation method that was used to determine Terrain corrections is based on elevation values on a grid of latitude and longitude.

Table 2.1 Density and magnetic susceptibility table of collected rock samples from the survey area.

Station	Sample	Formation	Density (g/cm³)	Magnetic Susceptibility (*10^-3 s.i)
13RB340A	Fine Grained Sandstone	Cuchara Formation	2.27	0.047
13RB340B	Coarse-Grained Sandstone	Cuchara Formation	2.23	0.045
13RB341	Fine-Grained Sandstone	Cuchara Formation	2.34	13.3
13RB342	Porphyritic Dike	Granodiorite	2.57	12.1
13RB343	Porphyritic Dike	Granodiorite	2.81	21.8
13RB344A	Conglomerate	Poison Canyon Formation	2.48	0.375
13RB344B	Porphyritic Dike	Syenogabro	2.72	25.4
13RB346A	Sill	Syenodiorite	2.53	15.9
13RB346B	Black Shale	Poison Canyon Formation	1.66	0.092
13RB347A	Siltstone	Vermejo Formation	2.17	0.093
13RB347B	Shale	Vermejo Formation	2.52	0.247
13RB347C	Sandstone	Vermejo Formation	2.48	0.154
13RB349A	Porphyritic Dike	Granodiorite	2.67	11.4
13RB349B	Black Shale	Cuchara Formation	2.55	0.229
13RB349C	Shale	Cuchara Formation	2.44	0.571
13RB381A	Sandstone	Raton Formation	2.26	0.478
13RB381B	Coal	Raton Formation	1.63	0.047
13RB381C	Siltstone	Raton Formation	2.32	0.171
13RB392A	Fine-Grained Sandstone	Sangre de Cristo Formation	2.8	0.143
13RB392B	Coarse-Grained Sandstone	Sangre de Cristo Formation	2.44	0.225
13RB392C	Coarse-Grained Sandstone	Sangre de Cristo Formation	2.48	0.135
13RB401	A metamorphic unit	Gneiss	2.52	0.212
13RB418	Porphyritic Dike	Syenodiorite	2.67	11.8

Table 2.1 continued.

Station	Sample	Formation	Density (g/cm³)	Magnetic Susceptibility (*10^-3 s.i)
14R07C	Red and Green variegated siltstone	Morrison Formation	2.19	0.082
14R06A	Fine-Grained Sandstone	Dakota Sandstone	2.34	0.071
14R04A	Grey Coarse-Grained Sandstone	Poison Canyon Formation	2.41	1.71
14R17A	A Metamorphic Cobble	Gneiss	2.69	0.246
14R11B	Fine Grained Sandstone	Sangre de Cristo Formation	2.39	0.324
14R07A	Greenish Sandstone	Morrison Formation	2.47	0.154
14R02A	Coarse-Grained Reddish Sandstone	Cuchara Formation	2.38	0.103
14R08A	Coarse-Grained Sandstone	Dockum Group	2.44	0.202
14R10A	Red and Orange Fine-Grained Sandstone	Entrada Sandstone	2.35	0.656
14R07B	Chert/Mudstone	Morrison Formation	2.14	0.75
14R03A	Grey Sandstone	Poison Canyon Formation	2.45	14.7
14R09A	Coarse-Grained Maroon Sandstone	Dockum Group	2.39	0.851
14R11A	Coarse-Grained Sandstone	Sangre de Cristo Formation	2.51	0.281
14R03B	Porphyritic Dike	Granite	2.69	7.96
14R05A	Grey Shale	Pierre Shale	2.38	2.75
14R01A	Sandstone	Cuchara Formation	2.31	0.191
14R01B	Porphyritic Dike	Andesite	2.65	7.29
14R16A	A Cobble of Foliated Quartzite	Quartzite	2.72	0.159

Deviation on data base points may occur. Therefore, each point should be determined by interpolation of the surrounding data base points. Interpolated terrain correction was added to Bouguer gravity anomaly. Sum of the interpolated terrain corrections and Bouguer gravity anomalies are concluded by complete Bouguer anomaly. Completed Bouguer anomaly was used to gravity interpretations. Differences between interpolated Bouguer anomaly plot and simple Bouguer anomaly plot are shown in figure 2.3.

This study intends to gain valuable interpretations about geologic features of the basin. Hence, pre-existed gravity data was used to produce another cross-section to compare with our gravity anomaly profile. This cross-section was considered to cut our gravity anomaly profile and provide us more data for understanding subsurface geology of the survey area. Structural models were built by cross-sections. These models are the foremost components of the study and will be discussed following chapters.

Figure 2.3. A) Free-Air anomaly. B) Simple Bouguer anomaly. C) Complete Bouguer anomaly.

2.2. Introduction of Field Work for Magnetic Survey

Magnetic anomaly surveys show us variations in the Earth's magnetic field caused by variations in the induced and remnant magnetism components of the rocks. In this study, the main purpose of the magnetic survey is to detect dikes. Magnetic survey was performed by Geometrics G-846 proton magnetometer. The survey, representing 414 measurements within every 10 feet, locations of stations are shown on figure 2.3.

Geometric G-846 proton magnetometer is a portable instrument and usually used for ground magnetic measurements (Figure 2.4).Its precision is 1-5 nT. It is convenient to measure magnetic signatures along parallel lines cover the survey area. The magnetometer can be operated by single person. However, another person may be needed for surveying or grid layout (Mariita, 2007). Man-made structures create intense magnetic fields on the survey point and cause a problem in magnetic surveys. All kind of ferrous metals around a magnetometer can easily deflect the data. The compass and belt buckles should be removed while a magnetic survey occurs (Mariita, 2007).

Data recording methods vary according to the purpose of a survey. Our method includes recording 3-5 readings, and averaging the result. Then, another five readings are taken ten feet away, and averaging the result. Some important features recorded in the field book for such as station numbers, time, weather and man-made structures after each reading. Anomalies were calculated based on differences from IGRF11 values as calculated from the NDAA (NGDC) online calculator.

After all corrections have been made, magnetic survey data are usually displayed as individual profiles or as contour maps. Identification of anomalies caused by man-made structures such as railroads, pipelines, and bridges should be shown on the maps.

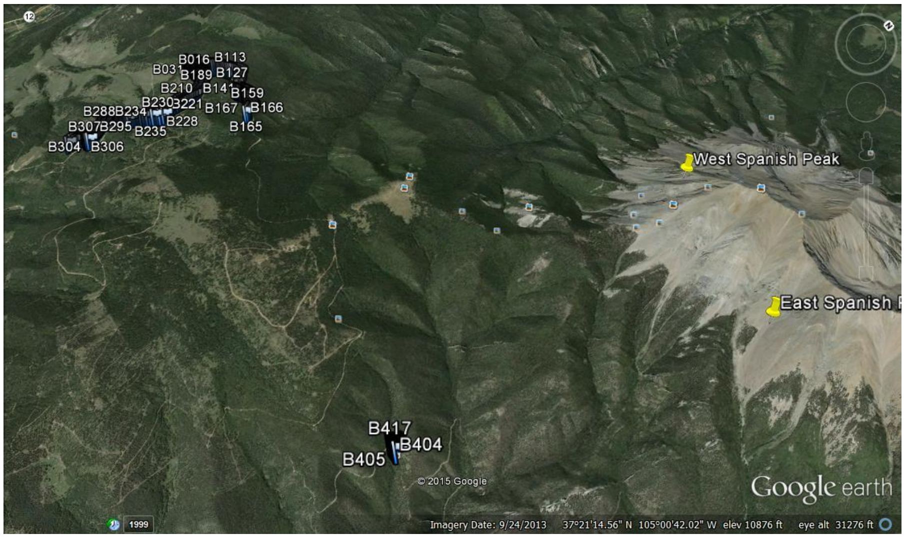

Figure 2.4. Google Earth image showing location of magnetic reading stations and the Spanish Peaks.

Figure 2.5. Geometric G-846 proton magnetometer was used to collect magnetic anomaly readings during fieldwork.

2.2.1. Magnetic Susceptibility

Magnetic anomalies are the result of variations in magnetic susceptibility and remnant magnetism of Earth materials. In order to constrain our models we have measured magnetic susceptibility of the Raton basin rocks.

We used the Terraplus K-10 Magnetic Susceptibility Meter to measure magnetic susceptibility values of our rock samples (Figure 2.5). Three different measurements were taken for accurate measurement, and errors calculated base on the standard deviations. Magnetic susceptibility measurements is shown in table 2.1 (Appendix A).

Presence of rocks with either high magnetic susceptibility or high remnant magnetism in the subsurface possibly causes for magnetic highs. Igneous and metamorphic rocks generally have high magnetic susceptibility. Sedimentary rocks have lower magnetic susceptibility compared with igneous and metamorphic rocks (Mariita, 2007). Magnetic surveys often are undertaken to better identify subsurface geologic structures.

Figure 2.6. Terraplus K-10 Magnetic Susceptibility Meter was used to measure magnetic susceptibilities of rock samples.

CHAPTER 3

STRUCTURAL MODELLING

3.1 Introduction

Gravity and magnetic data has been gathered across the Raton basin. Gravity modeling has done to obtain more knowledge about geologic features of the basin while magnetic modeling has done for the dikes. All corrections on gravity data were applied. Density values of rocks samples were measured. Also, magnetic susceptibility measurements have been accomplished. Consequently, all relevant and reliable geologic information that can help to improve the study was collected from previous studies.

A key part of understanding the geologic implications of potential filed data is to build quantitative models. Gravity and magnetic models has not been built only to understand geology of the basin but also provide basic knowledge about tectonic frameworks of the Raton basin.

The GRAVMAG software was used to produce 2D gravity and magnetic models. GRAVMAG calculates the gravity and magnetic signature of north sided polygons. These polygons can be graphically shaped into potential geologic configurations and compared to observational data. The 2-D models project the polygons to an infinite distance perpendicular from the profile.

3.2. Data Preparation

Our collected data was merged with pre-existing data from the University of Texas, El Paso National Gravity and Magnetic database. The resulting data was gridded to produce the map below. Gravity stations and geologic features of the basin such as faults and dikes are shown on Simple Bouguer gravity anomaly map (Figure 3.1). Furthermore, magnetic readings are represented by regional magnetic anomaly map (Figure 3.2).

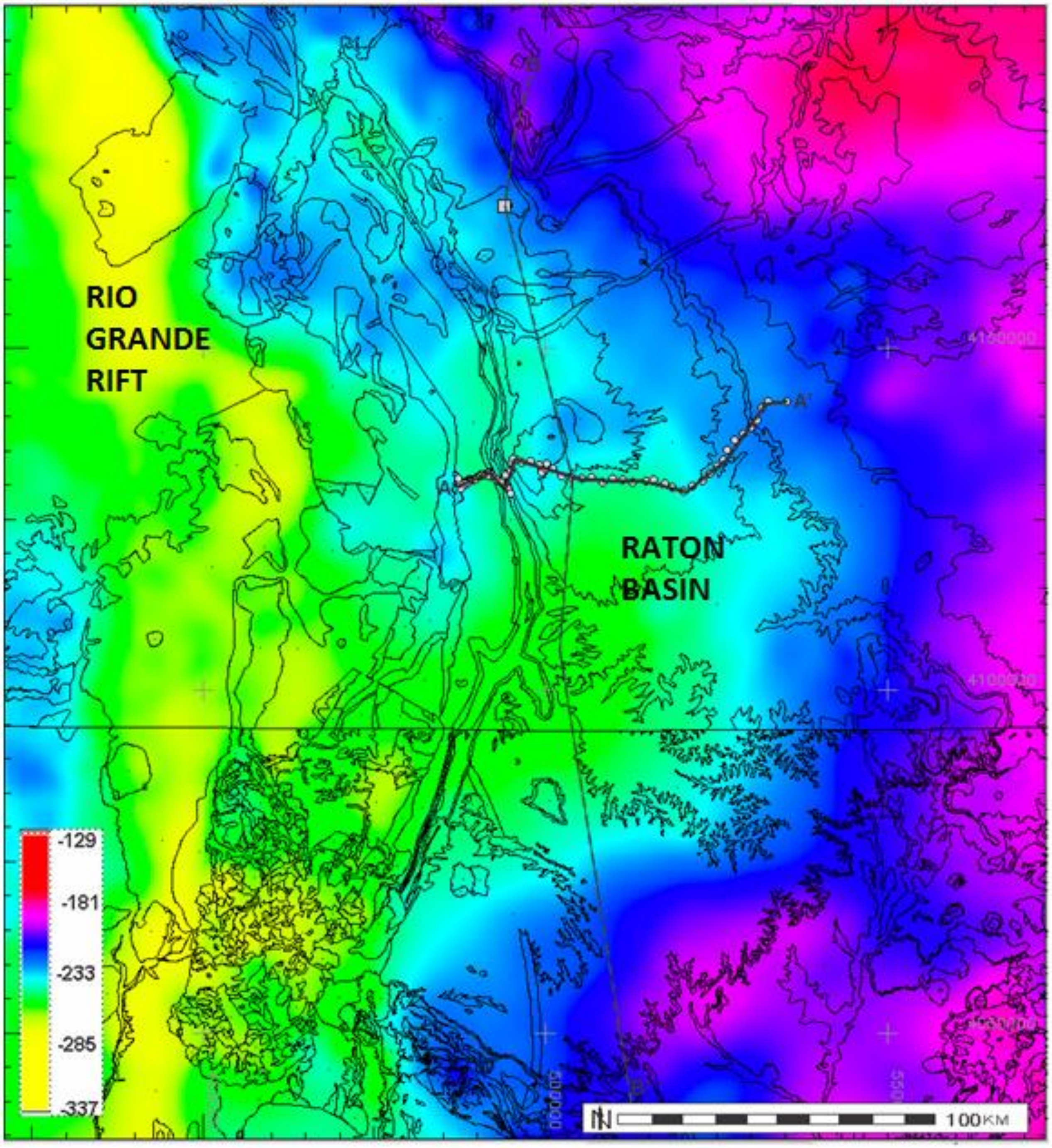

Figure 3.1. Regional gravity anomaly map of the Raton Basin with the orientations of the cross-section A-A'and B-B' (White dots indicate our measurements).

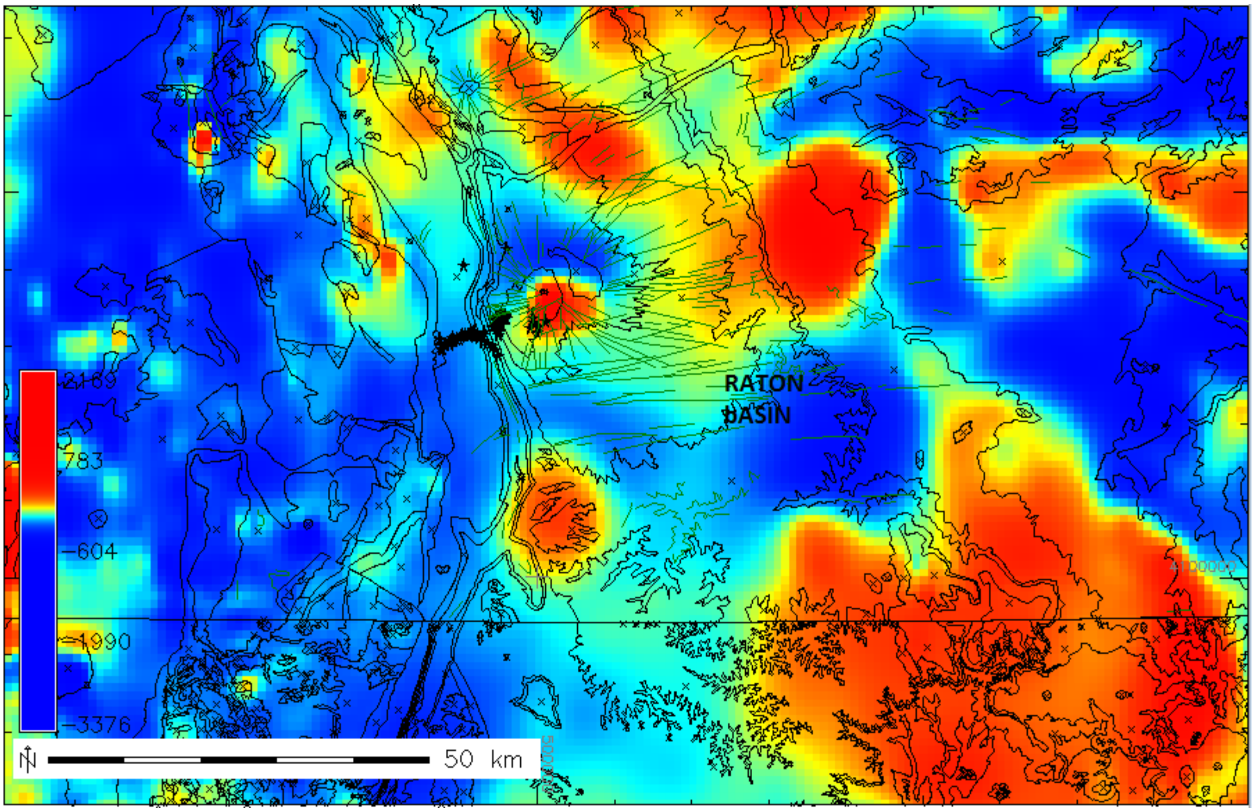

Figure 3.2. Regional magnetic anomaly map of the Raton Basin showing magnetic reading stations (Black dots indicate our measurements).

3.3. Orientation of the Cross-Sections

Orientations of the gravity cross-sections were different from orientation of the magnetic cross-sections. Orientations of magnetic cross-sections built based on distribution of dikes and topographic conditions. Distinctively, gravity sections were perpendicular to each other.

3.4. Building Cross-Sections

3.4.1. Gravity Cross-Sections

Quantitative 2-D gravity models of the Raton Basin were produced in order to better understand its geology. These models are constrained by observational gravity data. GRAVMAG was used to build gravity models. As mentioned in the previous chapter, orientations of cross sections (A-A’ and B-B’) were determined as the first step. A-A’ profile is perpendicular to the basin while B-B’ profile parallel to basin strike. A-A’ is along the gravity transect where B-B’ is constrained by the Freeman 3-24 drill core. Freeman 3-4 drill provides information about basin depth and geologic sequence. According to Freeman 3-24 drill core, thickness of sedimentary units is as deep as 3 km. A syncline axis coincides with the drilling point. A-A’ and B-B’ cross-sections are intersected. At that point, the two models have identical geometry. At the intersection point, the depth of the sedimentary units is almost 3 km for each models. Furthermore, each models cut the Raton formation at the intersection point. Rock densities measured in laboratory were imported to the GRAVMAG for gravity modeling. Three different density values were taken into account as average density values for three types of rocks. Density value for basement rocks was considered as the average. Density value for intrusive rocks was taken 0.1 g/cm^3 higher than density value of basement rocks. Also, density value for sedimentary rocks was accepted 0.4 g/cm^3 lower than density value of basement rocks. Existing geologic observations and drill core data (Freeman 3-24) was helpful to build initial model geometries. As the final step, bodies that correspond to geologic rock units were added. Models were ready to be built and interpretation of geologic characteristics of the basin.

A-A’ cross-section follows the gravity transect and is approximately 48 km in length. The depth of the cross-section is 8 km. B-B’ cross-section is parallel to basin strike and intersect the A-A’ cross-section. The drill core data taken from Freeman 3-24 well was taken into account to assume prospective geometry and estimated depth of the basin for B-B’ cross-section (Figure 3.3). As I mentioned before, GRAVMAG works based on density differences between bodies while building gravity models. Density differences are considered same for all models. Density value is 2.8 g/cm^3 for igneous rocks, 2.3 g/cm^3 for sedimentary rocks and 2.7 g/cm^3 for basement rocks. Differences between them were used for modeling. Table 2.1 shows rock densities.

Overall range of the gravity readings are between -224 to -246 mGal. However, a correction of +200 mGal to all gravity readings to remove the effect of thickened crust. The goal of the model is to better understand upper crustal Raton Basin and not overall crustal thickening due to the Laramide orogeny.

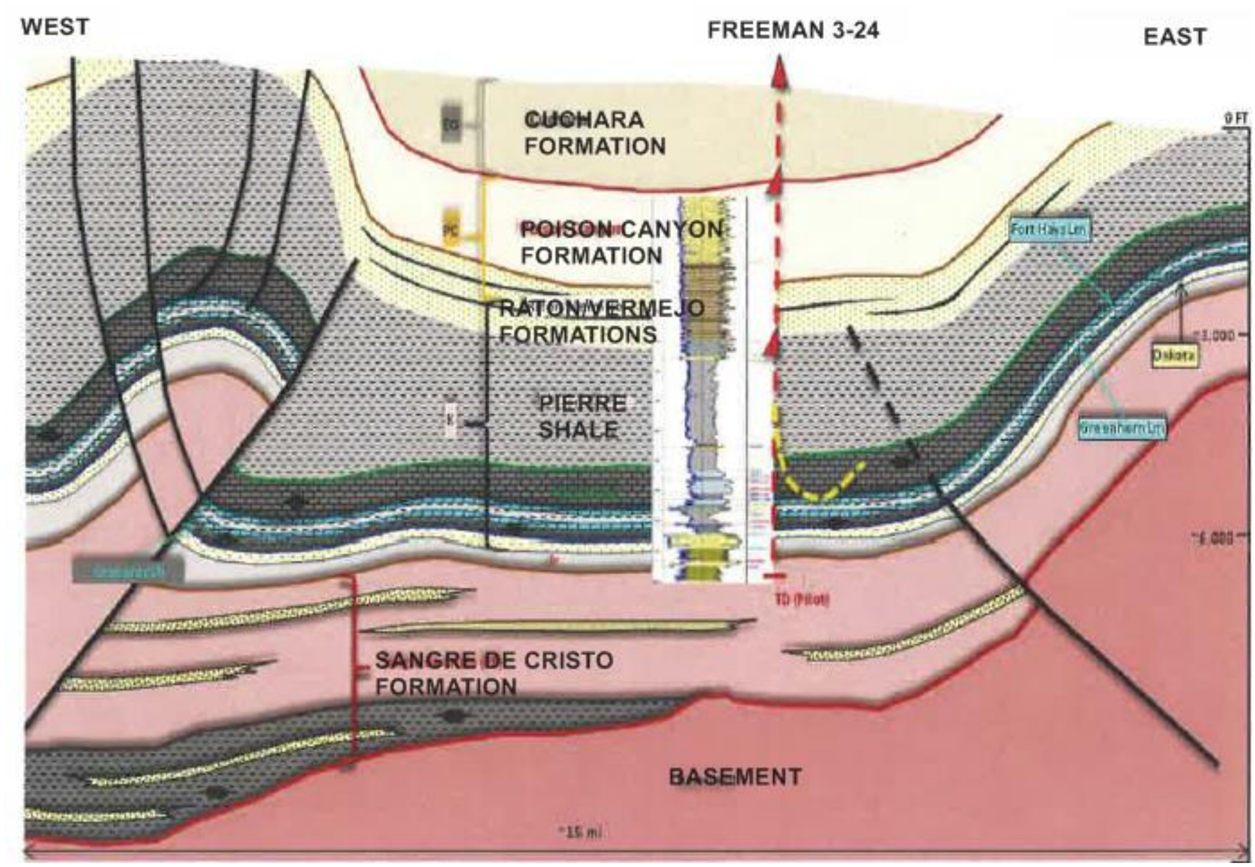

Figure 3.3. Conseptual cross-section of the Raton Basin south of the proposed Freeman 3-24 Well (Source: SWEPI) (taken from the paper named by Freeman 3-24 well Nontributary determination Huerfano County, Colorado Raton Basin prepared by AMEC Environmental & Infrastructure, INC., 2012).

3.4.1.1. A-A' Cross-Section

Laramide structure in the region is characterized by west to east compression and thrusting (Cordell and Keller, 1984). So, it is evident on the cross-section that a bunch of thrust faults on the western limit of the cross-section and one back-thrust on the eastern boundary of the cross-section are squeezed the sedimentary units. Previous geologic studies pointed out long north-south trending thrust faults might lie mainly to the west of the region. Whiskey Creek, Cuchara Pass, and Coal Creek Faults could be those thrust faults that were mentioned in previous studies (Johnson, 1968). Nappes appear on the western side due to thrusting. Thrust faults on the west trigger sedimentary rocks along the western edge of the basin to be extensively deformed because it has a steep eastward dip of the sedimentary rocks on the west limb.

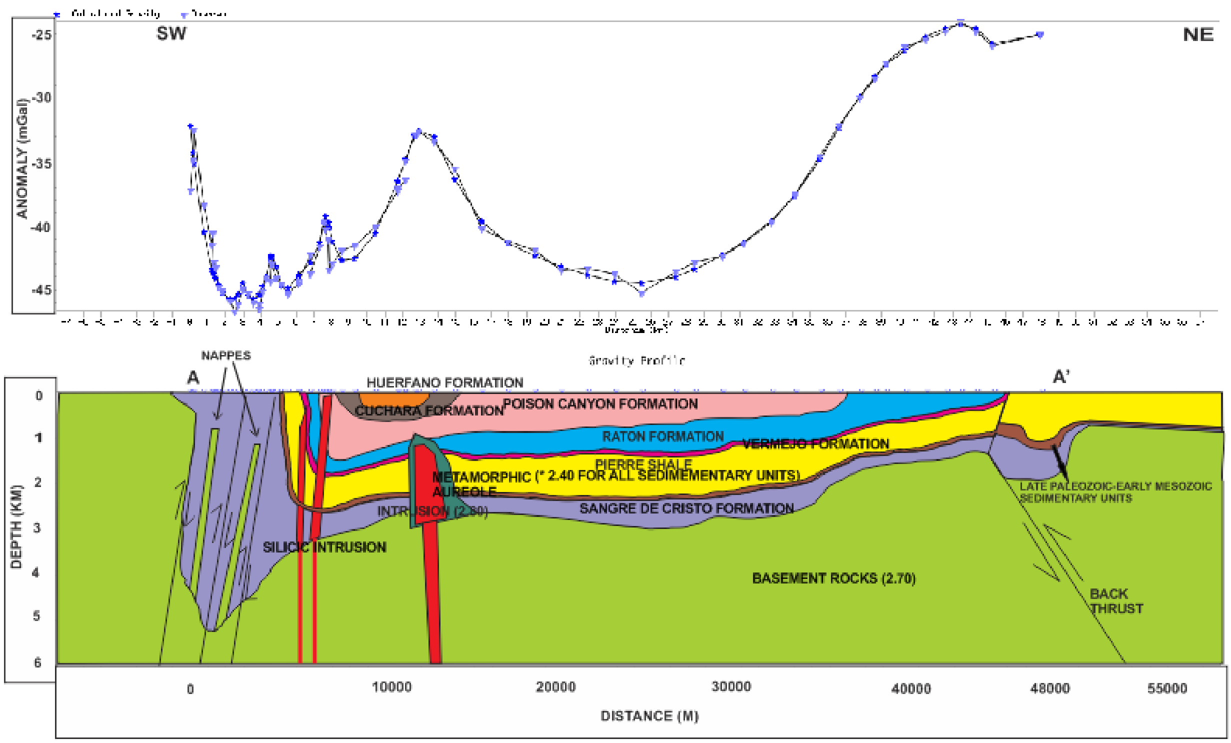

Figure 3.4. Gravity cross-section A-A'. Numbers in parentheses indicate density values used to build cross-sections.

Pennsylvanian age Sangre de Cristo Formation is the basal sedimentary unit in the survey area, and it comes out along the western side of the cross-section due to thrusting. It is overlain by late Mesozoic – early Cretaceous thin section of sedimentary units. Pierre shale covers them. Its thickness is 1.8-2.2 km. It is conformably overlain by late Cretaceous Trinidad sandstone and Vermejo formation. Both sedimentary units are cut by back thrust on the east of the cross-section. Late Cretaceous Raton formation overlies to the Vermejo formation. Thickness of the Raton formation is 1.3-1.8 km. The Raton formation is conformably overlain by Paleocene Poison Canyon formation. Eocene age Cuchara formation overlies the Poison canyon formation. At the top, Eocene age Huerfano formation covers the Cuchara formation. Its thickness is 300-400 m. Furthermore, there are sharp ascents between 6th to 18th km on the profile. They correspond to presence of intrusive rocks. The westernmost thin intrusions are silicic intrusions. Moreover, metamorphic aureole zone covers the easternmost intrusion. Metamorphic aureole indicates that contact metamorphism occurred in that area. After that point, the gravity anomalies start to decrease and the basin correspondingly deepens. The deepest portion of the basin after intrusion is almost 3 km. Thickness of Laramide orogenic sediments is 1.5-2 km.

3.4.1.2. B-B' Cross-Section

This cross section intersects the Freeman 3-24 well and cut through the A-A' cross-section (Figure 3.5). The reason of the orientation is to combine gravity and well log data. Geologic information was derived from Freeman 3-24 well, and applied to the B-B' cross-section. The length of the model is 170 km. The depth of the basin is taken 6 km same as the previous model. The purpose of this model is to gain much more understanding about geological and geophysical properties of the Raton Basin (Figure 3.6).

Two thrust faults on the northern limit of the basin and another normal fault at the southern edge of the basin are compressed the sedimentary units. Intersection point of the Freeman 3-24 well is located at 20th km. Intersection point correspond to an anticline axis..

According to the Freeman 3-24 well, Pennsylvanian age Sangre de Cristo formation is the basal sedimentary unit of the basin. The depth of Sangre de Cristo formation is 2.7 km at the intersection point of the Freeman 3-24 well. Cretaceous age Pierre shale comes out on the top of the Sangre de Cristo formation. The Sangre de Cristo formation and Pierre shale are significantly thicker in the southern part of the basin. The Trinidad sandstone overlies the Pierre shale. The Trinidad sandstone is a thin layer of fine-grained sandstone that is cut by a normal fault on the south. Late Cretaceous Raton formation overlies the Trinidad sandstone. Paleocene age Poison canyon formation overlies the Raton formation, and its depth is 1.8 – 2 km at the intersection of Freeman 3-24 well. The Poison Canyon formation is conformably overlain by Eocene Cuchara formation. The Cuchara formation appears just on the north of A-A' cross-section. Its depth is approximately 700-800 m. Eocene age Huerfano formation is at the top. Its depth is 300-400m. The maximum depth of the sedimentary units is 4.6- 5 km. Igneous rocks intruded sedimentary rocks between intersections of Freeman 3-24 well and A-A' cross-section.

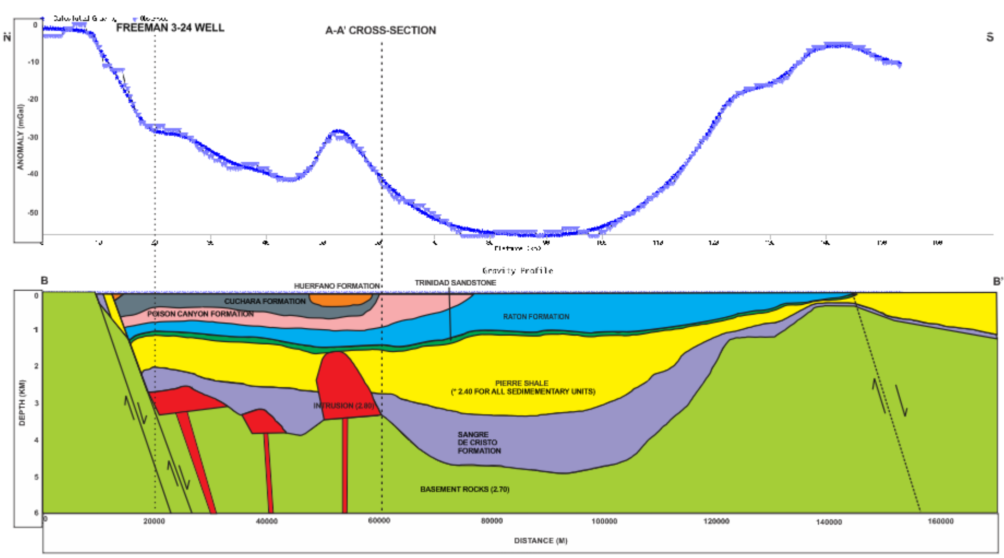

Figure 3.5. Gravity cross-section B-B'. Numbers in parentheses indicate density values used to build cross-sections.

3.4.2. Magnetic Cross-Sections

Magnetic anomalies collected in the field and magnetic susceptibilities of rock samples were used to produce the below magnetic models. The GRAVMAG program was used to build magnetic models. First, orientations of cross sections were designated. Two different profiles (C-C' and D-D') were taken from the whole profile. Second, magnetic anomaly readings and magnetic susceptibility values were imported to the GRAVMAG for magnetic modeling. Magnetic susceptibility meter measured magnetic susceptibilities of rock samples as the s.i unit. We had to convert the unit of susceptibility from s.i to cgs in order to use GRAVMAG for magnetic modeling. Converting formula are stated below:

1 cgs= 1 s.i ⁄ 4π

After converting magnetic susceptibility units, we used an average magnetic susceptibility value for all igneous rocks as 0.001 cgs. Remnant inclination and declination values were required to match the amplitude of observed magnetic anomalies. As the final step, a bunch of bodies were created correspond to dikes. Most of these dikes were observed in the field, but some were buried.

3.4.2.1. C-C' Cross-Section

Length of the C-C' cross section is approximately 700 m (Figure 3.7). This profile was created in order to find out dike locations and orientations. Sedimentary rocks and basement rocks ignored while preparing the cross section because the survey area is characterized by radial dike swarms and magnetic models would allow us to identify intrusive features of the Raton basin.

In this cross section, 5 dikes were defined (Figure 3.8). All dikes in this cross section show remnant inclination that causes positive magnetic anomalies. We observed westernmost two dikes on the cross-section during fieldwork. Rest of three dikes was probably buried and we couldn't see. The most prominent feature on the cross section, the easternmost dike is the highest one according to the data. The dike is highly magnetized. Other dikes are relatively low magnetized and mostly buried.

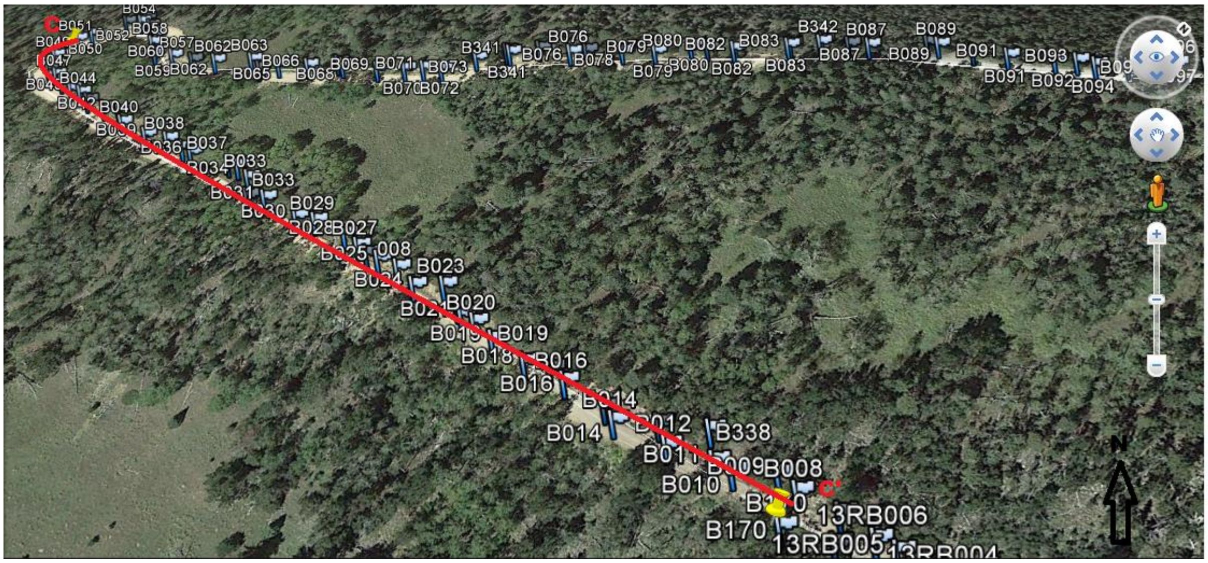

Figure 3.6. Orientation of C-C' cross section with magnetic stations (image was taken from Google Earth).

3.4.2.2. D-D' Cross-Section

Length of the D-D' cross section is approximately 1400 m (Figure 3.9). This cross section is longer than the C-C' cross section. This profile was also created in order to find out dike locations and orientations. Sedimentary rocks and basement rocks ignored as well.

In this cross section, we defined much more dikes rather than D-D' cross section (Figure 3.10). Since orientation of the cross section is roughly perpendicular to the Spanish Peaks. Dikes in this cross section show both remnant inclination and remnant declination. The easternmost four dikes show characteristics of radial dike swarms in the Raton basin. Dikes are highly magnetized. Consequently, show abrupt fluctuation on the profile.

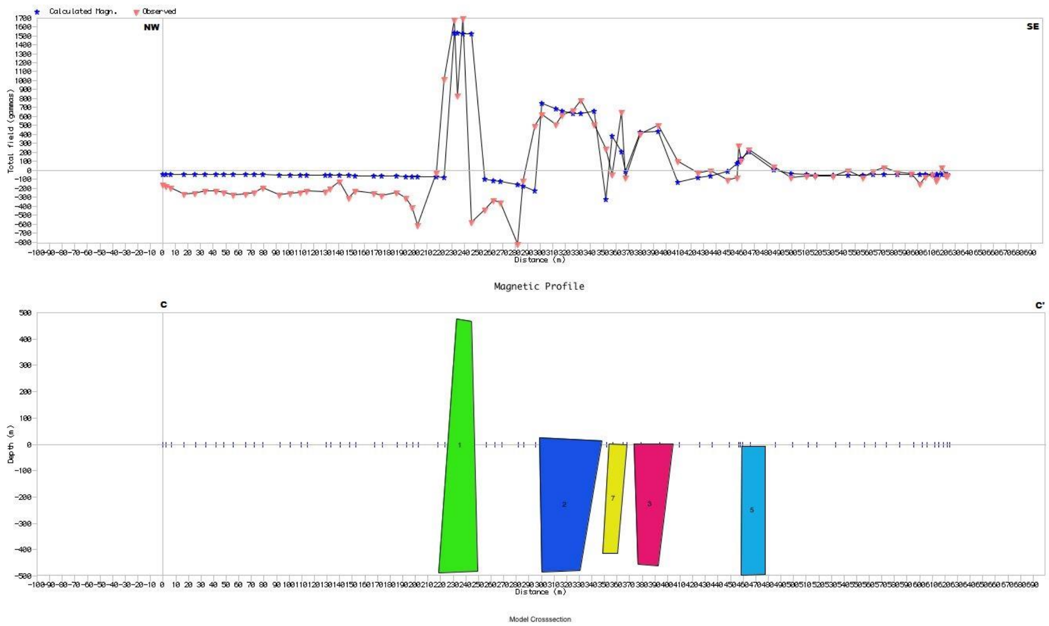

Figure 3.7. C-C' cross section. Total width of cross section is 700 m and total depth of the cross section is 500 m.

Figure 3.8. Orientation of D-D' cross section with magnetic stations (image was taken from Google Earth).

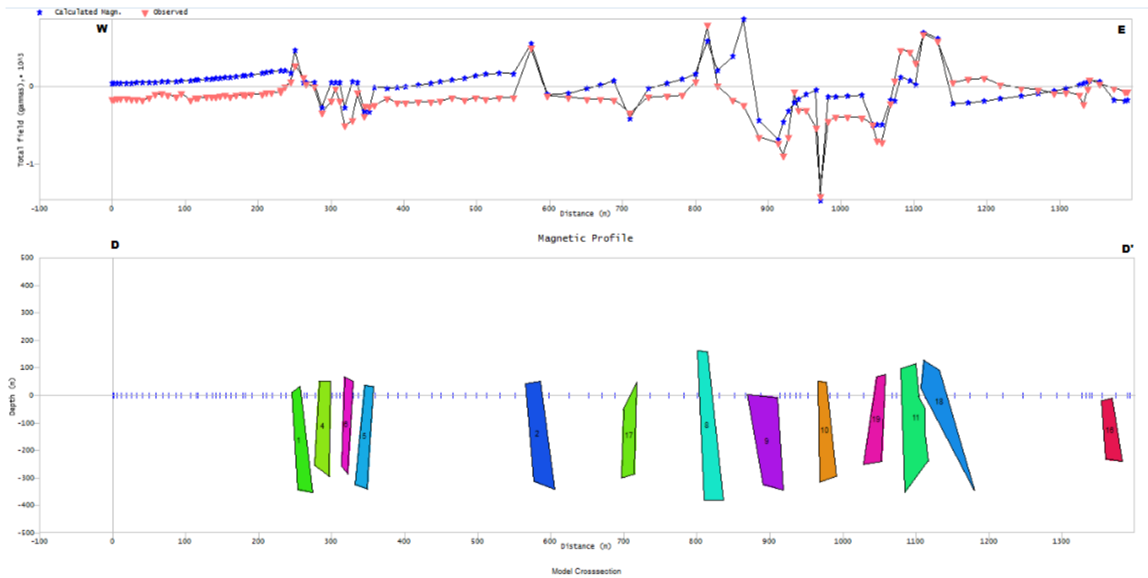

Figure 3.9. D-D' cross section. Total width of cross section is 1400 m and total depth of the cross section is 500 m.

CHAPTER 4

CONCLUSIONS

There have been a number of detailed geologic studies of the Raton basin. However, there have not previously been investigations that jointly interpreted geologic, gravity and magnetic observations, such has been done here. Therefore, this study concentrated on collecting as much geophysical data as possible in the fieldwork. We tried to reveal to tectonic frameworks and magmatic history of the Raton basin. To reach the purpose, gravity and magnetic survey has done, and structural models created in the GRAVMAG program. Conclusions of my thesis are listed below.

1) The Raton Basin is characterized by a significant negative Bouguer gravity anomaly. In the northern Raton basin the anomaly is approximately 20 mgal, whereas in the southern portion the negative anomaly is approximately 55-60 mgal.
2) Structurally, the Raton Basin is deformed into a highly asymmetric synform with shallow dips in the east and steep to overturned dips along its western limb. This synform is bounded by multiple high-angle reverse faults in the west, and contains a zone of structurally repeated nappes in the Sangre de Cristo Formation. Gravity models also indicate a forebulge and possibly an eastward vergent thrust fault at the eastern edge of the basin.
3) Gravity models, constrained by surface geology, drill core data, and rock density measurements, suggest that the Raton Basin thickens from approximately 3 km in the north to 5 km in the south.
4) The basin deepens at the central portion. Pennsylvanian Sangre de Cristo formation is the basal sedimentary unit of the basin, and it was thrusted at the western edge of the survey area. Accumulation of the Sangre de Cristo formation is related to the Ancestral Rocky

Mountains. After the Sangre de Cristo range uplifting and erosion, the Sangre de Cristo formation was formed. Sedimentary units that were accumulated from the late Cretaceous to the Tertiary time show continuous sequence in survey area. So, syn-Laramide orogenic sedimentation is continually represented in the survey area.

5) The Poison Canyon, Cuchara and Huefano Formations are syn-orogenic Laramide age units that were deposited in conjunction with the evolution of the La Veta Syncline and fill depositional space along the syncline axis.

6) The Raton Basin is also characterized by an approximately 10 mgal gravity high between the northern and southern parts. This high is associated with the Spanish Peaks. Gravity models indicate a high density magmatic intrusion underlays much of this area. This is consistent with the metamorphic rocks and small outcrops of intrusive rock that occur in this area.

7) The significantly greater thickness of the Sangre de Cristo Formation in the southern part of the Raton Basin suggests that it also may have been a large foreland basin during the earlier Ancestral Rocky Mountains and that it has remained a locus of tectonic activity over much of its history.

8) Magnetic susceptibility values of the Raton Basin igneous rocks are between $11*10^{-3}$ and $25*10^{-3}$ s.i. Magnetic susceptibility values represent induced magnetism. However, interpretation of magnetic signatures of igneous rocks is not possible without remnant magnetization. Furthermore, igneous rocks of the Raton Basin show both reverse and normal magnetic polarity.

APPENDIX A

DENSITY AND MAGNETIC SUSCEPTIBLITY TABLES

Latitude	Longitude	Elevation	Station	Sample	Formation	Density (g/cm³)	Magnetic Susceptibility (*10^-3 s.i)	S.Deviation
37.35	-105.06	3224.60	13RB340A	Fine Grained Sandstone	Cuchara Formation	2.27	0.05	0.00
37.35	-105.06	3224.60	13RB340B	Coarse-Grained Sandstone	Cuchara Formation	2.23	0.05	0.01
37.35	-105.06	3238.30	13RB341	Fine-Grained Sandstone	Cuchara Formation	2.34	13.30	0.78
37.35	-105.06	3241.40	13RB342	Porphyritic Dike	Granodiorite	2.57	12.10	0.46
37.35	-105.05	3297.40	13RB343	Porphyritic Dike	Granodiorite	2.81	21.80	1.16
37.35	-105.05	3304.60	13RB344A	Conglomerate	Poison Canyon Formation	2.48	0.38	0.03
37.35	-105.05	3304.60	13RB344B	Porphyritic Dike	Syenogabro	2.72	25.40	0.15
37.34	-105.06	3108.30	13RB346A	Sill	Syenodiorite	2.53	15.90	0.60
37.34	-105.06	3108.30	13RB346B	Black Shale	Poison Canyon Formation	1.66	0.09	0.01
37.34	-105.06	3096.00	13RB347A	Siltstone	Vermejo Formation	2.17	0.09	0.01
37.34	-105.06	3096.00	13RB347B	Shale	Vermejo Formation	2.52	0.25	0.20
37.34	-105.06	3096.00	13RB347C	Sandstone	Vermejo Formation	2.48	0.15	0.02

Latitude	Longitude	Elevation	Station	Sample	Formation	Density (g/cm³)	Magnetic Susceptibility (*10^-3 s.i)	S.Deviation
37.33	-105.07	3062.90	13RB349A	Porphyritic Dike	Granodiorite	2.67	11.40	1.19
37.33	-105.07	3062.90	13RB349B	Black Shale	Cuchara Formation	2.55	0.23	0.02
37.33	-105.07	3062.90	13RB349C	Shale	Cuchara Formation	2.44	0.57	0.08
37.43	-105.04	2364.00	13RB381A	Sandstone	Raton Formation	2.26	0.48	0.01
37.43	-105.04	2364.00	13RB381B	Coal	Raton Formation	1.63	0.05	0.00
37.43	-105.04	2364.00	13RB381C	Siltstone	Raton Formation	2.32	0.17	0.02
37.33	-105.11	2791.80	13RB392A	Fine-Grained Sandstone	Sangre de Cristo Formation	2.80	0.14	0.01
37.33	-105.11	2791.80	13RB392B	Coarse-Grained Sandstone	Sangre de Cristo Formation	2.44	0.23	0.02
37.33	-105.11	2791.80	13RB392C	Coarse-Grained Sandstone	Sangre de Cristo Formation	2.48	0.14	0.00
37.34	-105.00	3042.00	13RB401	A metamorphic unit	Gneiss	2.52	0.21	0.01
37.34	-105.00	3073.00	13RB418	Porphyritic Dike	Syenodiorite	2.67	11.80	0.31
37.35	-105.05	3267.70	14R07C	Red and Green variegated siltstone	Morrison Formation	2.19	0.08	0.00

Latitude	Longitude	Elevation	Station	Sample	Formation	Density (g/cm³)	Magnetic Susceptibility (*10^-3 s.i)	S.Deviation
37.40	-104.65	2945.39	14R06A	Fine-Grained Sandstone	Dakota Sandstone	2.34	0.07	0.01
37.38	-104.67	2980.42	14R04A	Grey Coarse-Grained Sandstone	Poison Canyon Formation	2.41	1.71	0.02
37.34	-105.01	3332.08	14R17A	A Metamorphic Cobble	Gneiss	2.69	0.25	0.00
37.32	-105.07	30251.62	14R11B	Fine Grained Sandstone	Sangre de Cristo Formation	2.39	0.32	0.01
37.35	-105.05	3267.70	14R07A	Greenish Sandstone	Morrison Formation	2.47	0.15	0.01
37.36	-104.70	3013.41	14R02A	Coarse-Grained Reddish Sandstone	Cuchara Formation	2.38	0.10	0.01
37.35	-105.04	3364.72	14R08A	Coarse-Grained Sandstone	Dockum Group	2.44	0.20	0.01
37.32	-105.07	3031.63	14R10A	Red and Orange Fine-Grained Sandstone	Entrada Sandstone	2.35	0.66	0.09
37.35	-105.05	3267.70	14R07B	Chert/Mudstone	Morrison Formation	2.14	0.75	0.01
37.38	-104.69	3002.21	14R03A	Grey Sandstone	Poison Canyon Formation	2.45	14.70	0.12
37.35	-105.03	3430.25	14R09A	Coarse-Grained Maroon Sandstone	Dockum Group	2.39	0.85	0.04

Latitude	Longitude	Elevation	Station	Sample	Formation	Density (g/cm³)	Magnetic Susceptibility (*10^-3 s.i)	S.Deviation
37.33	-105.04	3345.72	14R11A	Coarse-Grained Sandstone	Sangre de Cristo Formation	2.51	0.28	0.04
37.38	-104.69	3002.21	14R03B	Porphyritic Dike	Granite	2.69	7.96	0.33
37.39	-104.66	2956.78	14R05A	Grey Shale	Pierre Shale	2.38	2.75	0.33
37.35	-104.71	3041.72	14R01A	Sandstone	Cuchara Formation	2.31	0.19	0.01
37.35	-104.71	3041.72	14R01B	Porphyritic Dike	Andesite	2.65	7.29	0.44
37.35	-105.03	3430.25	14R16A	A Cobble of Foliated Quartzite	Quartzite	2.72	0.16	0.00

APPENDIX B

GRAVITY READINGS

Station	Latitude	Longitude	UTM northing	UTM easting	Elevation (MSL) EGM96	Elevation error (m)	Dial reading	Daily Base Avg.	Mgal from base	Absolute gravity (mgal)	Calculated Gravity (sea level)	Free-Air gravity correction	Simple Bouguer gravity correction	Free-Air Anomaly	Simple Bouguer Anomaly	Easting distance from 13RB 370 (m)	Interpolated Terrain Correction	Spherical cap correction	Complete Bouguer Anomaly
13RB 352	37.3317033	-105.0970343	4131674.74	491403.92	2820.66	0.1	1172.8	1172.25	0.05	979128.8	979934.5107	870.454133	316.4157165	64.75	-251.67	4082.83	6.471911	1.31	-246.50
13RB 353	37.3302829	-105.0994485	4131517.39	491189.88	2836.65	0.1	1125.5	1172.25	-3.95	979124.86	979934.3868	875.39019	318.2100052	65.86	-252.35	3868.79	6.171204	1.30	-247.48
13RB 354	37.32968748	-105.1024598	4131517.38	491189.878	2851.36	0.2	1086.5	1172.25	-7.24	979121.5673	979934.3349	879.9290788	319.8599207	67.16	-252.70	3868.79	6.171204	1.29	-247.82
13RB 355	37.32956514	-105.1060267	4131451.62	490923.04	2870.95	0.2	1051.3	1172.25	-10.21	979118.60	979934.3242	885.9757872	322.0579384	70.25	-251.81	3601.95	5.778541	1.28	-247.31
13RB 356	37.32926557	-105.1094212	4131438.39	490607.034	2892.49	0.1	1012.4	1172.25	-13.49	979115.31	979934.2981	892.6211796	324.4735815	73.64	-250.84	3285.95	5.547794	1.27	-246.56
13RB 357	37.32766477	-105.1123138	4131405.5	490306.268	2907.83	0.3	979.1	1172.25	-16.30	979112.50	979934.1586	897.3560294	326.1947301	75.70	-250.49	2985.18	5.547794	1.26	-246.20
13RB 358	37.32549487	-105.1147187	4131228.21	490049.807	2925.21	0.2	924.9	1172.25	-20.88	979107.93	979933.9694	902.7210404	328.1449464	76.68	-251.47	2728.72	5.336978	1.25	-247.38
13RB 359	37.32420167	-105.1176619	4130987.74	489836.458	2946.28	0.2	867.5	1172.25	-25.72	979103.08	979933.8566	909.222008	330.5080902	78.45	-252.06	2515.37	5.336978	1.23	-247.96
13RB 360	37.32347999	-105.1222009	4130844.59	489575.523	2979.41	0.3	791.5	1172.25	-32.14	979096.67	979933.7937	919.4462346	334.2246628	82.32	-251.90	2254.44	6.009191	1.21	-247.11
13RB 361	37.32348673	-105.12512	4130765.04	489173.274	3000.07	0.2	743.7	1172.25	-36.17	979092.63	979933.7943	925.8203676	336.5417015	84.66	-251.88	1852.19	6.784893	1.20	-246.30
13RB 362	37.32331167	-105.1269765	4130766.13	488914.654	3021.07	0.3	697.5	1172.25	-40.07	979088.74	979933.779	932.3031278	338.8982268	87.26	-251.64	1593.57	6.784893	1.19	-246.04
13RB 363	37.32125311	-105.1279194	4130746.92	488750.14	3044.24	0.2	644.6	1172.25	-44.53	979084.27	979933.5996	939.4521554	341.4969446	90.12	-251.37	1429.05	8.091222	1.17	-244.45

Station	Latitude	Longitude	UTM northing	UTM easting	Elevation (MSL) EGM 96	Elevation error (m)	Dial reading	Daily Base Avg.	Mgal from base	Absolute gravity (mgal)	Calculated Gravity (sea level)	Free-Air gravity correction	Simple Bouguer gravity correction	Free-Air Anomaly	Simple Bouguer Anomaly	Easting distance from 13RB370 (m)	Interpolated Terrain Correction	Spherical cap correction	Complete Bouguer Anomaly
13 RB 365	37.31877396	-105.1283211	4130453	488582.076	3084.35	0.5	544.3	1172.25	-53.00	979075.81	979933.3835	951.8310272	345.9967447	94.25	-251.74	1260.99	10.26021	1.14	-242.62
13 RB 366	37.31905498	-105.1342986	4130243.67	488630.334	3133.25	0.2	441.2	1172.25	-61.70	979067.10	979933.408	966.919407	351.4814685	100.62	-250.87	1309.25	10.26021	1.11	-241.71
13 RB 367	37.31652653	-105.1372969	4130275.59	488100.746	3176.12	0.2	338.7	1172.25	-70.35	979058.45	979933.1875	980.1503234	356.2909924	105.42	-250.88	779.66	12.49649	1.07	-239.45
13 RB 368	37.31265423	-105.1404071	4129566.28	487558.466	3218.58	0.5	232.1	1172.25	-79.35	979049.46	979932.85	993.2531708	361.0539623	109.86	-251.19	237.38	18.7443	1.04	-233.49
13 RB 369	37.31876523	-105.1412198	4130244.34	487487.459	3214.38	0.4	264	1172.25	-76.66	979052.15	979933.3827	991.9585938	360.5833752	110.72	-249.86	166.37	14.98934	1.04	-235.91
13 RB 370	37.32475511	-105.1431089	4130909.1	487321.086	3193.16	0.2	326.1	1172.25	-71.42	979057.39	979933.9049	985.4082502	358.2022828	108.89	-249.31	0.00	12.04328	1.06	-238.32
13 RB 371							1171.7	1172.25	-0.05	979128.76	978032.6771								
13 RB 372	37.33280515	-105.094902	4131796.79	491592.941	2828.50	0.2	1167.6	1172.25	-0.39	979128.41	979934.6067	872.8744828	317.2955293	66.68	-250.62	4271.85	6.471911	1.30	-245.45
13 RB 373	37.33294839	-105.0914355	4131812.38	491900.038	2857.66	0.2	1112.2	1172.25	-5.07	979123.74	979934.6192	881.8729502	320.5665305	70.99	-249.58	4578.95	6.619564	1.29	-244.24
13 RB 374	37.3311228	-105.0910497	4131609.81	491934.017	2874.56	0.6	1070.9	1172.25	-8.55	979120.25	979934.46	887.089216	322.4626769	72.88	-249.58	4612.93	6.619564	1.28	-244.24
13 RB 375	37.32964956	-105.0881369	4131446.13	492191.906	2894.60	0.5	1017.5	1172.25	-13.06	979115.74	979934.3316	893.2723256	324.7102773	74.68	-250.03	4870.82	5.912086	1.27	-245.38
13 RB 376	37.32874852	-105.0917363	4131346.47	491872.939	2916.64	0.6	963.2	1172.25	-17.64	979111.16	979934.253	900.0757212	327.1833557	76.98	-250.20	4551.85	5.912086	1.25	-245.54
13 RB 377	37.32695818	-105.0850173	4131147.3	492468.011	2954.52	0.3	869.7	1172.25	-25.54	979103.27	979934.097	911.7645634	331.4323256	80.94	-250.50	5146.92	5.921334	1.23	-245.80
13 RB 378	37.3228802	-105.0807881	4130694.56	492842.297	2991.55	0.3	777	1172.25	-33.36	979095.45	979933.7414	923.1920214	335.5862806	84.90	-250.69	5521.21	5.349398	1.21	-246.55
13 RB 379	37.32048842	-105.0739042	4130428.72	493451.995	3031.33	0.1	689.2	1172.25	-40.77	979088.04	979933.5329	935.4696724	340.0492863	89.97	-250.08	6130.91	5.541683	1.18	-245.71
13 RB 380	37.31589873	-105.0663587	4129919.04	494120.18	2984.21	0.1	789.3	1172.25	-32.32	979096.48	979933.1328	920.9281318	334.7633421	84.28	-250.48	6799.09	6.752139	1.21	-244.94

Station	Latitude	Longitude	UTM northing	UTM easting	Elevation (MSL) EGM 96	Elevation error (m)	Dial reading	Daily Base Avg.	Mgal from base	Absolute gravity (mgal)	Calculated Gravity (sea level)	Free-Air gravity correction	Simple Bouguer gravity correction	Free-Air Anomaly	Simple Bouguer Anomaly	Easting distance from 13RB 370 (m)	Interpolated Terrain Correction	Spherical cap correction	Complete Bouguer Anomaly
13RB381	37.31204338	-105.0607128	4129491	494620.166	2920.28	0.1	935.3	1172.25	-20.00	979108.81	979932.7967	901.1971736	327.5910109	77.21	-250.38	7299.08	8.73777	1.25	-242.90
13RB382	37.30530523	-105.0580385	4128743.33	494856.682	2881.71	0.1	1020.5	1172.25	-12.81	979116.00	979932.2094	889.2966318	323.2650869	73.08	-250.18	7535.60	10.45902	1.27	-241.00
13RB393							1162.7	1162.7	0.00	979128.80	978032.6771								
13RB394							681.5	1162.7	-40.61	979088.19	978032.6771								
13RB395	37.3300308	-105.0665061	4131486.86	494108.226	3052.38	0.4	638.1	1162.7	-44.28	979084.53	979934.3648	941.9641594	342.4100744	92.13	-250.28	6787.14	7.995175	1.16	-243.45
13RB396	37.33536104	-105.056753	4132077.63	494972.607	3095.09	0.2	545.2	1162.7	-52.12	979076.69	979934.8296	955.1450826	347.2014253	97.00	-250.20	7651.52	9.879972	1.13	-241.45
13RB397	37.34634376	-105.054782	4133295.94	495147.907	3180.17	0.5	359.1	1162.7	-67.82	979060.98	979935.7872	981.400462	356.7454258	106.59	-250.15	7826.82	9.088744	1.07	-242.13
13RB398	37.3520162	-105.054161	4133925.21	495203.27	3260.24	0.3	156.2	1162.7	-84.95	979043.86	979936.2818	1006.110064	365.7275263	113.68	-252.04	7882.18	8.6676	1.00	-244.38
13RB399	37.34992061	-105.0463718	4133692.36	495893.002	3305.00	0.5	58	1162.7	-93.24	979035.57	979936.0991	1019.923	370.748618	119.39	-251.36	8571.92	9.41041	0.96	-242.91
13RB400	37.3377449	-105.0064175	4132340.6	499431.533	3279.71	0.6	131.5	1162.7	-87.03	979041.77	979935.0374	1012.118506	367.9116338	118.85	-249.06	12110.45	12.62742	0.99	-237.42
13RB401	37.34359444	-105.0108516	4132989.58	499038.833	3331.52	0.1	17.4	1162.7	-96.66	979032.14	979935.5475	1028.105529	373.7230203	124.70	-249.02	11717.75	11.97838	0.94	-237.99
13RB402	37.33316285	-105.0062981	4131832.27	499442.076	3178.36	0.2	379.1	1162.7	-66.14	979062.67	979934.6379	980.840353	356.5418226	108.87	-247.67	12120.99	12.72076	1.07	-236.02
13RB403	37.33884601	-105.0000138	4132462.74	499998.774	3097.53	0.8	603.6	1162.7	-47.19	979081.62	979935.1334	955.896215	347.4744668	102.38	-245.10	12677.69	12.25215	1.13	-233.97

Station	Latitude	Longitude	UTM northing	UTM easting	Elevation (MSL) EGM96	Elevation error (m)	Dial reading	Daily Base Avg.	Mgal from base	Absolute gravity (mgal)	Calculated Gravity (sea level)	Free-Air gravity correction	Simple Bouguer gravity correction	Free-Air Anomaly	Simple Bouguer Anomaly	Easting distance from 13RB 370 (m)	Interpolated Terrain Correction	Spherical cap correction	Complete Bouguer Anomaly
13RB 431	37.34571124	-104.9975111	4133224.37	500220.442	2999.76	0.4	842.5	1162.7	-27.02	979101.78	979935.732	925.7271704	336.5078237	91.77	-244.73	12899.36	12.07894	1.20	-233.85
13RB 432	37.33880528	-104.987753	4132458.29	501084.836	2888.96	1	1098.7	1162.7	-5.40	979123.40	979935.1299	891.5318216	324.0775929	79.80	-244.27	13763.75	10.87101	1.27	-234.67
13RB 433	37.32924868	-104.9743328	4131398.32	502273.885	2776.45	0.9	1377.8	1162.7	18.15	979146.96	979934.2966	856.8115442	311.4565471	69.47	-241.98	14952.80	6.503009	1.33	-236.81
13RB 434	37.32775288	-104.9574352	4131232.92	503770.928	2666.72	0.2	366.8	-78.1	37.55	979166.35	979934.1662	822.9507178	299.1479173	55.14	-244.01	16449.84	3.761557	1.38	-241.63
13RB 435	37.32602506	-104.9408752	4131042.03	505238.143	2593.98	0.2	532.2	-78.1	51.51	979180.31	979934.0156	800.5019194	290.9876337	46.80	-244.19	17917.06	2.945127	1.41	-242.65
13RB 436	37.32623756	-104.9235727	4131066.7	506771.035	2535.12	0.1	664	-78.1	62.63	979191.44	979934.0341	782.3383406	284.3850551	39.74	-244.64	19449.95	2.690989	1.43	-243.38
13RB 437	37.32064345	-104.9067401	4130447.43	508262.924	2469.04	0.2	795.5	-78.1	73.73	979202.54	979933.5464	761.945744	276.9722141	30.94	-246.04	20941.84	2.546744	1.45	-244.94
13RB 438	37.32472584	-104.8899449	4130901.93	509750.471	2421.84	0.2	910.6	-78.1	83.45	979212.25	979933.9023	747.3785896	271.6769591	25.73	-245.95	22429.39	2.600554	1.46	-244.81
13RB 439	37.32349565	-104.8728645	4130767.35	511263.92	2375.58	2.2	1015	-78.1	92.26	979221.06	979933.7951	733.103988	266.488049	20.37	-246.12	23942.83	2.364197	1.48	-245.23
13RB 440	37.31986131	-104.8556459	4130366.35	512790.065	2330.11	0.3	1102.7	-78.1	99.66	979228.46	979933.4783	719.0716374	261.3871986	14.06	-247.33	25468.98	2.081814	1.49	-246.73
13RB 441	37.32222565	-104.8341522	4130631.78	514693.983	2278.30	0.2	1246.8	-78.1	111.82	979240.63	979933.6844	703.0836886	255.5754757	10.03	-245.55	27372.90	1.922438	1.49	-245.12
13RB 442	37.32339823	-104.8217512	4130763.86	515792.459	2255.41	0.1	1312.4	-78.1	117.36	979246.16	979933.7866	696.0192174	253.0074946	8.40	-244.61	28471.37	1.74555	1.50	-244.36
13RB 443	37.31897024	-104.8041885	4130275.7	517349.496	2215.68	0.1	268.5	-1218.5	125.50	979254.31	979933.4006	683.7582308	248.5505466	4.67	-243.89	30028.41	1.557865	1.50	-243.83
13RB 444	37.31310879	-104.7905916	4129628.02	518555.668	2190.07	0.1	334.7	-1218.5	131.09	979259.89	979932.8896	675.8552934	245.6777776	2.86	-242.82	31234.58	1.427133	1.50	-242.90
13RB 445	37.30871234	-104.7728128	4129143.92	520132.219	2142.55	0.1	463.2	-1218.5	141.94	979270.74	979932.5064	661.19093	240.3471865	-0.58	-240.92	32811.13	1.198846	1.51	-241.23

Station	Latitude	Longitude	UTM northing	UTM easting	Elevation (MSL) EGM96	Elevation error (m)	Dial reading	Daily Base Avg.	Mgal from base	Absolute gravity (mgal)	Calculated Gravity (sea level)	Free-Air gravity correction	Simple Bouguer gravity correction	Free-Air Anomaly	Simple Bouguer Anomaly	Easting distance from 13RB 370 (m)	Interpolated Terrain Correction	Spherical cap correction	Complete Bouguer Anomaly
13RB 446	37.3150218	-104.758219	4129847.1	521423.668	2122.61	0.1	544.6	-1218.5	148.81	979277.61	979933.0564	655.0371374	238.110243	-0.41	-238.52	34102.58	0.941534	1.51	-239.09
13RB 447	37.32241138	-104.7421608	4130670.65	522844.307	2099.93	0.1	642	-1218.5	157.03	979285.83	979933.7006	648.0390152	235.5663803	0.17	-235.40	35523.22	0.902653	1.51	-236.00
13RB 448	37.3322158	-104.7300229	4131761.36	523916.614	2070.48	0.1	746	-1218.5	165.80	979294.61	979934.5553	638.948585	232.26195	-1.00	-233.26	36595.53	1.102767	1.51	-233.67
13RB 449	37.34086321	-104.7168531	4132724.11	525080.421	2055.84	0.1	811.4	-1218.5	171.32	979300.13	979935.3093	634.432224	230.6202235	-0.75	-231.37	37759.33	1.396305	1.51	-231.48
13RB 450	37.34976405	-104.7068964	4133714.26	525959.294	2041.72	0.1	868.7	-1218.5	176.16	979304.96	979936.0854	630.0757178	229.0366053	-1.05	-230.08	38638.21	1.649982	1.51	-229.94
13RB 451	37.36266323	-104.6998513	4135147.26	526578.709	2013.41	0.2	960.6	-1218.5	183.92	979312.72	979937.2103	621.3386346	225.860619	-3.15	-229.01	39257.62	1.725514	1.51	-228.80
13RB 452	37.37511951	-104.6880665	4136532.55	527617.713	2002.21	0.1	1016.3	-1218.5	188.62	979317.42	979938.2967	617.8813888	224.6038877	-2.99	-227.60	40296.63	1.57291	1.51	-227.53
13RB 453	37.3845033	-104.6745314	4137577.65	528812.485	1980.42	0.1	1086.7	-1218.5	194.56	979323.36	979939.1153	611.1579206	222.1598635	-4.59	-226.75	41491.40	1.325271	1.51	-226.94
13RB 454	37.39261459	-104.6617498	4138481.5	529940.768	1956.78	0.1	1160.5	-1218.5	200.79	979329.59	979939.8228	603.8619994	219.5077488	-6.37	-225.88	42619.68	1.079279	1.51	-226.30
13RB 455	37.40250871	-104.6520542	4139582.29	530794.948	1945.39	0.2	1209.4	-1218.5	204.91	979333.72	979940.686	600.3464282	218.2298159	-6.62	-224.85	43473.86	0.830565	1.51	-225.52
13RB 456	37.41766164	-104.6424271	4141266.56	531640.624	1933.87	0.2	1244.8	-1218.5	207.90	979336.71	979942.0082	596.7928992	216.9380851	-8.51	-225.45	44319.54	0.638305	1.50	-226.31
13RB 457	37.42651812	-104.6315758	4142252.81	532596.984	1916.10	0.1	1283.8	-1218.5	211.19	979340.00	979942.781	591.3096944	214.9449047	-11.47	-226.42	45275.90	0.514809	1.50	-227.41
13RB 458	37.42638438	-104.6013096	4142248.87	535274.916	1886.79	0.1	1364	-1218.5	217.96	979346.77	979942.7693	582.2621596	211.6560671	-13.74	-225.40	47953.83	0.414672	1.50	-226.48
14R12							1692.7			979128.80									
14R13.cor	37.32050047	-105.0738655	4130430.05	493455.429	3031.63	0.1	1211.2			979088.17	979933.534	935.559475	340.0819301	90.19	-249.89	6134.34	5.541683	1.18	-245.53

Station	Latitude	Longitude	UTM northing	UTM easting	Elevation (MSL) EGM96	Elevation error (m)	Dial reading	Daily Base Avg.	Mgal from base	Absolute gravity (mgal)	Calculated Gravity (sea level)	Free-Air gravity correction	Simple Bouguer gravity correction	Free-Air Anomaly	Simple Bouguer Anomaly	Easting distance from 13RB370 (m)	Interpolated Terrain Correction	Spherical cap correction	Complete Bouguer Anomaly
14R14.cor	37.35133426	-105.0527689	4133849.49	495326.519	3267.70	0.1	668.7			979042.38	979936.2224	1008.410677	366.563814	114.57	-252.00	8005.43	9.044854	1.00	-243.95
14R15.cor	37.34604126	-105.0381503	4133261.66	496620.979	3364.72	0.6	437.5			979022.87	979935.7608	1038.353826	377.4483428	125.46	-251.99	9299.89	10.41646	0.91	-242.48
14R16.cor	37.34843056	-105.0251865	4133526.34	497769.272	3430.25	0.1	300.6			979011.31	979935.9692	1058.573607	384.798364	133.92	-250.88	10448.19	10.79385	0.85	-240.94
14R17.cor	37.34362495	-105.0109231	4132992.97	499032.495	3332.08	0.2	543.8			979031.84	979935.5501	1028.280814	373.7867374	124.57	-249.22	11711.41	11.97838	0.94	-238.18
14R18	37.32050047	-105.0738655	4130430.05	493455.429	3031.63	0.1	1209.3			979088.01	979933.534	935.559475	340.0819301	90.03	-250.05	6134.34	5.541683	1.18	-245.69

APPENDIX C

MAGNETIC READINGS

Latitude	Longitude	UTM easting	UTM Northing	Stations	Distance East from RB51	Altitude	Total Field Value	Base Station Value	Corrected Total Field	Anomaly
37.313728	-105.139038			13RB002	367.83	3208				
37.331841	-105.097273			13RB003	357.02	2846.8				
37.348839	-105.057576	494900.61	4133572.91	13RB004	351.89	3202.3	51,088	51,002	86	-78
37.348838	-105.057698	494889.81	4133572.81	13RB005	342.59	3219.1	51,116	51,002	114	-50
37.348834	-105.057756	494884.67	4133572.37	13RB006	332.22	3220.3	51,404	51,002	402	239
37.34884	-105.057861	494875.37	4133573.04	13RB007	326.20	3220.5	51,678	51,002	676	513
37.348829	-105.057978	494865.01	4133571.82	13RB008	317.52	3221	51,948	51,002	946	783
37.34884	-105.058046	494858.98	4133573.05	13RB009	312.47	3221.5	51,838	51,002	836	673
37.348794	-105.058144	494850.30	4133567.95	13RB010	301.04	3221.2	51,780	51,002	778	615
37.34879	-105.058201	494845.25	4133567.51	13RB011	295.46	3222	51,680	51,002	678	515
37.34876	-105.05833	494833.83	4133564.19	13RB012	286.34	3222.4	51,788	51,002	786	623
37.348791	-105.058393	494828.25	4133567.63	13RB013	281.82	3223.2	51,660	51,002	658	495
37.348738	-105.058496	494819.12	4133561.76	13RB014	268.45	3222.9	51,048	51,002	46	-118
37.348754	-105.058547	494814.61	4133563.53	13RB015	262.87	3223.4	50,344	51,002	-658	-822
37.348749	-105.058698	494801.23	4133562.99	13RB016	256.22	3222.2	50,803	51,002	-199	-363
37.348754	-105.058761	494795.65	4133563.55	13RB017	245.24	3222.7	50,828	51,002	-174	-338
37.34873	-105.058836	494789.01	4133560.89	13RB018	238.24	3222.7	50,728	51,002	-274	-438
37.348722	-105.05896	494778.03	4133560.01	13RB019	234.44	3222.4	50,588	51,002	-414	-578
37.348722	-105.059039	494771.03	4133560.01	13RB020		3222.4	52,862	51,002	1,860	1,697
37.348713	-105.059082	494767.22	4133559.01	13RB021		3222.2	51,998	51,002	996	833

Latitude	Longitude	UTM easting	UTM Northing	Stations	Distance East from RB51	Altitude	Total Field Value	Base Station Value	Corrected Total Field	Anomaly
37.348722	-105.059113	494764.47	4133560.01	13RB022	231.69	3223.4	52,843	51,002	1,841	1,678
37.348742	-105.059204	494756.42	4133562.24	13RB023	223.63	3223.4	52,186	51,002	1,184	1,021
37.348692	-105.059272	494750.39	4133556.70	13RB024	217.61	3223.6	51,137	51,002	135	-29
37.348693	-105.059446	494734.98	4133556.82	13RB025	202.20	3223.6	50,553	51,002	-449	-613
37.348687	-105.059494	494730.73	4133556.15	13RB026	197.94	3223.4	50,754	51,002	-248	-412
37.34869	-105.059547	494726.03	4133556.49	13RB027	193.25	3223.9	50,856	51,002	-146	-310
37.348699	-105.059632	494718.51	4133557.49	13RB028	185.72	3224.4	50,920	51,002	-82	-246
37.34868	-105.059762	494706.99	4133555.39	13RB029	174.21	3223.6	50,888	51,002	-114	-278
37.348659	-105.059832	494700.79	4133553.07	13RB030	168.01	3224.6	50,913	51,002	-89	-253
37.34865	-105.060001	494685.82	4133552.08	13RB031	153.04	3224.6	50,937	51,002	-65	-229
37.348625	-105.06006	494680.59	4133549.31	13RB032	147.81	3225.1	50,862	51,002	-140	-304
37.34867	-105.060142	494673.33	4133554.30	13RB033	140.55	3225.8	51,037	51,002	35	-129
37.348682	-105.060229	494665.63	4133555.64	13RB034	132.85	3225.1	50,964	51,002	-38	-202
37.348671	-105.060267	494662.26	4133554.42	13RB035	129.48	3225.3	50,931	51,002	-71	-235
37.348632	-105.060441	494646.85	4133550.10	13RB036	114.07	3225.6	50,937	51,002	-65	-229
37.348629	-105.060491	494642.42	4133549.77	13RB037	109.64	3226.3	50,919	51,002	-83	-247
37.348622	-105.060588	494633.83	4133549.00	13RB038	101.05	3226.5	50,908	51,002	-94	-258
37.348594	-105.060684	494625.32	4133545.90	13RB039	92.54	3227.2	50,897	51,002	-105	-269
37.348581	-105.060835	494611.95	4133544.47	13RB040	79.17	3227	50,967	51,002	-35	-199
37.348605	-105.060911	494605.22	4133547.14	13RB041	72.44	3228.2	50,917	51,002	-85	-249

Latitude	Longitude	UTM easting	UTM Northing	Stations	Distance East from RB51	Altitude	Total Field Value	Base Station Value	Corrected Total Field	Anomaly
37.348586	-105.060988	494598.40	4133545.03	13RB042	65.62	3228.4	50,905	51,002	-97	-261
37.348576	-105.0611	494588.48	4133543.93	13RB043	55.70	3228.9	50,895	51,002	-107	-271
37.348584	-105.061183	494581.13	4133544.82	13RB044	48.34	3228.7	50,919	51,002	-83	-247
37.348578	-105.061252	494575.02	4133544.16	13RB045	42.23	3229.4	50,937	51,002	-65	-229
37.348582	-105.061348	494566.51	4133544.61	13RB046	33.73	3229.9	50,934	51,002	-68	-232
37.348595	-105.061439	494558.46	4133546.06	13RB047	25.67	3229.4	50,908	51,002	-94	-258
37.348602	-105.061542	494549.33	4133546.84	13RB048	16.55	3230.1	50,898	51,002	-104	-268
37.348664	-105.061655	494539.33	4133553.72	13RB049	6.55	3230.4	50,970	51,002	-32	-196
37.348715	-105.061701	494535.26	4133559.38	13RB050	2.48	3229.9	50,987	51,002	-15	-179
37.348772	-105.061729	494532.78	4133565.71	13RB051	0.00	3229.9	51,002	51,002	0	-164
37.348819	-105.061712	494534.29	4133570.92	13RB052		3230.4	51,006	51,002	4	-160
37.348929	-105.06166	494538.91	4133583.12	13RB053		3230.4	51,014	51,002	12	-152
37.34896	-105.061599	494544.31	4133586.56	13RB054		3231.6	51,013	51,002	11	-153
37.34896	-105.061516	494551.66	4133586.55	13RB055		3232.3	51,015	51,002	13	-151
37.348942	-105.061432	494559.10	4133584.55	13RB056		3232.8	51,010	51,002	8	-156
37.348922	-105.06136	494565.48	4133582.33	13RB057		3232.8	51,001	51,002	-1	-165
37.348872	-105.061267	494573.71	4133576.78	13RB058		3233.7	50,999	51,002	-3	-167
37.348837	-105.061157	494583.45	4133572.89	13RB059		3234.2	51,023	51,002	21	-143
37.348859	-105.061064	494591.69	4133575.32	13RB060		3234.5	51,070	51,002	68	-96
37.348882	-105.060958	494601.08	4133577.87	13RB061		3234.7	51,087	51,002	85	-79

Latitude	**Longitude**	**UTM easting**	**UTM Northing**	**Stations**	**Distance East from RB51**	**Altitude**	**Total Field Value**	**Base Station Value**	**Corrected Total Field**	**Anomaly**
37.348921	-105.060867	494609.14	4133582.19	13RB062		3235.7	51,057	51,002	55	-109
37.348993	-105.060744	494620.04	4133590.17	13RB063		3236.1	51,044	51,002	42	-122
37.348982	-105.060668	494626.77	4133588.95	13RB064		3236.1	51,085	51,002	83	-81
37.349027	-105.060618	494631.20	4133593.94	13RB065		3236.4	51,458	51,002	456	293
37.349079	-105.060519	494639.97	4133599.70	13RB066		3236.4	50,994	51,002	-8	-172
37.349144	-105.060435	494647.42	4133606.91	13RB067		3236.1	51,032	51,002	30	-134
37.349145	-105.060406	494649.99	4133607.01	13RB068		3236.4	51,030	51,002	28	-136
37.349197	-105.060276	494661.50	4133612.78	13RB069		3237.1	51,040	51,002	38	-126
37.349246	-105.060187	494669.39	4133618.21	13RB070		3237.3	51,036	51,002	34	-130
37.349281	-105.06013	494674.44	4133622.09	13RB071		3237.3	51,043	51,002	41	-123
37.349309	-105.060066	494680.11	4133625.19	13RB072		3237.8	51,051	51,002	49	-115
37.349389	-105.059982	494687.56	4133634.06	13RB073		3238.5	51,056	51,002	54	-110
37.349455	-105.059905	494694.38	4133641.38	13RB074		3239	51,040	51,002	38	-126
37.349522	-105.059817	494702.18	4133648.81	13RB075		3240	51,063	51,002	61	-103
37.349567	-105.059713	494711.39	4133653.79	13RB076		3240.5	51,067	51,002	65	-99
37.349603	-105.059676	494714.67	4133657.78	13RB077		3240.7	51,064	51,002	62	-102
37.349671	-105.059574	494723.71	4133665.32	13RB078		3240.5	51,067	51,002	65	-99
37.349728	-105.059478	494732.22	4133671.64	13RB079		3240.9	51,187	51,002	185	22
37.349817	-105.059403	494738.87	4133681.51	13RB080		3240.2	51,068	51,002	66	-98
37.349838	-105.059347	494743.83	4133683.84	13RB081		3240.2	51,096	51,002	94	-70

Latitude	Longitude	UTM easting	UTM Northing	Stations	Distance East from RB51	Altitude	Total Field Value	Base Station Value	Corrected Total Field	Anomaly
37.349876	-105.059264	494751.18	4133688.05	13RB082		3240.9	51,095	51,002	93	-71
37.349988	-105.059127	494763.32	4133700.47	13RB083		3241.4	51,102	51,002	100	-64
37.349998	-105.059126	494763.41	4133701.57	13RB084		3242.1	51,127	51,002	125	-39
37.350073	-105.059054	494769.79	4133709.89	13RB085		3242.4	51,168	51,002	166	3
37.3501	-105.058964	494777.77	4133712.88	13RB086		3243.3	51,234	51,002	232	69
37.350131	-105.058905	494782.99	4133716.32	13RB087		3244.1	51,441	51,002	439	276
37.35026	-105.058764	494795.49	4133730.62	13RB088		3244.8	51,290	51,002	288	125
37.350265	-105.058724	494799.03	4133731.17	13RB089		3245.3	51,197	51,002	195	32
37.350272	-105.058594	494810.55	4133731.94	13RB090		3246	51,164	51,002	162	-2
37.350298	-105.058482	494820.47	4133734.82	13RB091		3245.8	50,827	51,002	-175	-339
37.350341	-105.058339	494833.14	4133739.58	13RB092		3247	50,983	51,002	-19	-183
37.350362	-105.058275	494838.81	4133741.91	13RB093		3247	51,144	51,002	142	-22
37.350362	-105.058212	494844.39	4133741.91	13RB094		3247.9	50,981	51,002	-21	-185
37.350423	-105.058133	494851.39	4133748.67	13RB095		3248.2	50,666	51,002	-336	-500
37.350496	-105.058014	494861.93	4133756.76	13RB096		3249.4	50,740	51,002	-262	-426
37.350521	-105.05793	494869.37	4133759.53	13RB097		3249.6	51,089	51,002	87	-77
37.350568	-105.05783	494878.23	4133764.74	13RB098		3250.3	50,787	51,002	-215	-379
37.350627	-105.057814	494879.65	4133771.28	13RB099		3250.8	50,918	51,002	-84	-248
37.350707	-105.057749	494885.42	4133780.16	13RB100		3251.3	50,905	51,002	-97	-261
37.350752	-105.057669	494892.50	4133785.14	13RB101		3252.7	50,926	51,002	-76	-240

Latitude	Longitude	UTM easting	UTM Northing	Stations	Distance East from RB51	Altitude	Total Field Value	Base Station Value	Corrected Total Field	Anomaly
37.35087	-105.057477	494909.52	4133798.22	13RB102		3253	51,016	51,002	14	-150
37.350941	-105.05732	494923.43	4133806.09	13RB103		3253.4	50,961	51,002	-41	-205
37.350999	-105.057182	494935.65	4133812.52	13RB104		3253.9	50,964	51,002	-38	-202
37.351106	-105.056997	494952.04	4133824.38	13RB105		3254.9	50,977	51,002	-25	-189
37.351196	-105.056792	494970.21	4133834.35	13RB106		3256.1	50,976	51,002	-26	-190
37.351252	-105.056648	494982.96	4133840.56	13RB107		3257.3	50,985	51,002	-17	-181
37.351339	-105.056469	494998.82	4133850.20	13RB108		3259	51,029	51,002	27	-137
37.351417	-105.056279	495015.65	4133858.84	13RB109		3259.7	50,996	51,002	-6	-170
37.351517	-105.056102	495031.34	4133869.93	13RB110		3260.4	51,024	51,002	22	-142
37.351585	-105.055948	495044.98	4133877.46	13RB111		3261.1	51,011	51,002	9	-155
37.351712	-105.055739	495063.50	4133891.54	13RB112		3262.3	51,033	51,002	31	-133
37.351876	-105.05551	495083.79	4133909.73	13RB113		3263.8	51,032	51,002	30	-134
37.352014	-105.055242	495107.54	4133925.02	13RB114		3265.5	51,670	51,002	668	505
37.352146	-105.054989	495129.95	4133939.65	13RB115		3266.2	51,051	51,002	49	-115
37.352183	-105.054667	495158.47	4133943.74	13RB116		3267.6	51,033	51,002	31	-133
37.352185	-105.054379	495183.98	4133943.95	13RB117		3269.1	51,008	51,002	6	-158
37.352002	-105.054169	495202.56	4133923.63	13RB118		3270.3	51,010	51,002	8	-156
37.351771	-105.053966	495220.53	4133898.00	13RB119		3271.2	50,996	51,002	-6	-170
37.351694	-105.053713	495242.93	4133889.44	13RB120		3273.4	50,837	51,002	-165	-329
37.351554	-105.053423	495268.60	4133873.90	13RB121		3274.4	51,035	51,002	33	-131
37.351441	-105.053134	495294.19	4133861.35	13RB122		3275.8	51,045	51,002	43	-121

Latitude	Longitude	UTM easting	UTM Northing	Stations	Distance East from RB51	Altitude	Total Field Value	Base Station Value	Corrected Total Field	Anomaly
37.351315	-105.052903	495314.64	4133847.36	13RB123		3276.8	51,059	51,002	57	-107
37.351171	-105.052687	495333.76	4133831.37	13RB124		3277.7	51,238	51,002	236	73
37.350992	-105.052512	495349.25	4133811.50	13RB125		3278.4	51,966	51,002	964	801
37.350809	-105.052355	495363.15	4133791.19	13RB126		3279.4	51,180	51,002	178	15
37.350639	-105.052121	495383.86	4133772.32	13RB127		3280.8	50,997	51,002	-5	-169
37.35043	-105.05195	495398.99	4133749.13	13RB128		3282.5	50,925	51,002	-77	-241
37.350302	-105.051713	495419.97	4133734.91	13RB129		3285.4	50,520	51,002	-482	-646
37.350372	-105.051418	495446.11	4133742.67	13RB130		3287.6	50,439	51,002	-563	-727
37.350399	-105.051334	495453.55	4133745.66	13RB131		3288.3	50,278	51,002	-724	-888
37.35042	-105.051258	495460.28	4133747.98	13RB132		3289	50,514	51,002	-488	-652
37.350418	-105.051163	495468.69	4133747.76	13RB133		3289.5	51,109	51,002	107	-57
37.350436	-105.051096	495474.63	4133749.75	13RB134		3290.9	50,867	51,002	-135	-299
37.350424	-105.050978	495485.08	4133748.41	13RB135		3290.9	50,863	51,002	-139	-303
37.350537	-105.050762	495504.21	4133760.94	13RB136		3291.9	49,759	51,002	-1,243	-1,407
37.350494	-105.050827	495498.46	4133756.17	13RB137		3291.9	50,634	51,002	-368	-532
37.350584	-105.05064	495515.02	4133766.15	13RB138		3293.3	50,720	51,002	-282	-446
37.350631	-105.050529	495524.86	4133771.36	13RB139		3295.7	50,774	51,002	-228	-392
37.350706	-105.050343	495541.33	4133779.67	13RB140		3296.9	50,779	51,002	-223	-387
37.350748	-105.050122	495560.91	4133784.32	13RB141		3296.9	50,764	51,002	-238	-402
37.350803	-105.049944	495576.68	4133790.41	13RB142		3297.4	50,681	51,002	-321	-485
37.350772	-105.049889	495581.55	4133786.97	13RB143		3297.2	50,475	51,002	-527	-691

Latitude	Longitude	UTM easting	UTM Northing	Stations	Distance East from RB51	Altitude	Total Field Value	Base Station Value	Corrected Total Field	Anomaly
37.350762	-105.049801	495589.34	4133785.86	13RB144		3297.7	50,456	51,002	-546	-710
37.350758	-105.049677	495600.32	4133785.41	13RB145		3298.4	50,951	51,002	-51	-215
37.350752	-105.049609	495606.34	4133784.74	13RB146		3298.4	51,247	51,002	245	82
37.350726	-105.049514	495614.76	4133781.85	13RB147		3299.3	51,634	51,002	632	469
37.350694	-105.049377	495626.89	4133778.29	13RB148		3300.1	51,609	51,002	607	444
37.350691	-105.049285	495635.04	4133777.96	13RB149		3301	51,469	51,002	467	304
37.350682	-105.049169	495645.31	4133776.95	13RB150		3302	51,840	51,002	838	675
37.350628	-105.048936	495665.94	4133770.95	13RB151		3302.5	51,760	51,002	758	595
37.350508	-105.04871	495685.95	4133757.63	13RB152		3303.2	51,222	51,002	220	57
37.3504	-105.048474	495706.85	4133745.63	13RB153		3303.9	51,263	51,002	261	98
37.350286	-105.048224	495728.98	4133732.98	13RB154		3306.1	51,283	51,002	281	118
37.35023	-105.047969	495751.56	4133726.75	13RB155		3309.2	51,195	51,002	193	30
37.350163	-105.047654	495779.46	4133719.31	13RB156		3310.2	51,149	51,002	147	-17
37.350165	-105.047389	495802.93	4133719.52	13RB157		3311.1	51,126	51,002	124	-40
37.350182	-105.047134	495825.51	4133721.39	13RB158		3313.3	51,077	51,002	75	-89
37.350176	-105.046949	495841.90	4133720.72	13RB159		3314.2	51,096	51,002	94	-70
37.350138	-105.046749	495859.61	4133716.49	13RB160		3316.2	51,064	51,002	62	-102
37.350112	-105.046681	495865.63	4133713.60	13RB161		3316.4	50,939	51,002	-63	-227
37.350079	-105.046621	495870.94	4133709.94	13RB162		3316.9	51,140	51,002	138	-26
37.350043	-105.046588	495873.86	4133705.95	13RB163		3317.1	51,252	51,002	250	87
37.34989	-105.046432	495887.67	4133688.96	13RB164		3317.6	51,199	51,002	197	34

Latitude	Longitude	UTM easting	UTM Northing	Stations	Distance East from RB51	Altitude	Total Field Value	Base Station Value	Corrected Total Field	Anomaly
37.349699	-105.046216	495906.79	4133667.77	13RB165		3318.6	51,151	51,002	149	-15
37.349522	-105.046042	495922.19	4133648.12	13RB166		3320.3	51,102	51,002	100	-64
37.349296	-105.045995	495926.34	4133623.05	13RB167		3321.7	51,105	51,002	103	-61
37.348749	-105.057951	494867.39	4133562.95	13RB168			51,014	51,011	3	-152
37.348782	-105.057822	494878.82	4133566.60	13RB169			51,026	51,011	15	-140
37.348771	-105.057614	494897.24	4133565.37	13RB170	364.46	3057.3	51,813	51,011	802	648
37.348741	-105.057448	494911.94	4133562.03	13RB171	379.16	3064.1	51,569	51,011	558	404
37.34869	-105.057285	494926.37	4133556.36	13RB172	393.59	3072.7	51,666	51,011	655	501
37.348629	-105.057105	494942.31	4133549.59	13RB173	409.53	3079.9	51,266	51,011	255	101
37.348569	-105.056928	494957.99	4133542.92	13RB174	425.21	3081.8	51,141	51,011	130	-25
37.348516	-105.056814	494968.08	4133537.04	13RB175	435.30	3084.7	51,161	51,011	150	-5
37.348435	-105.056575	494989.24	4133528.04	13RB176	456.46	3087.4	51,081	51,011	70	-85
37.348466	-105.056658	494981.89	4133531.48	13RB177	449.11	3090	51,056	51,011	45	-110
37.348426	-105.056562	494990.39	4133527.04	13RB178	457.61	3092.2	51,439	51,011	428	274
37.348412	-105.05654	494992.34	4133525.48	13RB179	459.56	3096.5	51,275	51,011	264	110
37.348407	-105.056468	494998.72	4133524.93	13RB180	465.94	3102.3	51,399	51,011	388	234
37.348315	-105.056244	495018.55	4133514.71	13RB181	485.77	3106.1	51,203	51,011	192	38
37.348203	-105.056093	495031.92	4133502.27	13RB182	499.14	3108	51,083	51,011	72	-83
37.348115	-105.055952	495044.40	4133492.50	13RB183	511.62	3110.9	51,098	51,011	87	-68
37.34803	-105.055872	495051.48	4133483.07	13RB184	518.70	3112.1	51,103	51,011	92	-63
37.34793	-105.055709	495065.91	4133471.97	13RB185	533.13	3114.3	51,098	51,011	87	-68

Latitude	**Longitude**	**UTM easting**	**UTM Northing**	**Stations**	**Distance East from RB51**	**Altitude**	**Total Field Value**	**Base Station Value**	**Corrected Total Field**	**Anomaly**
37.347818	-105.05558	495077.33	4133459.54	13RB186	544.55	3115.7	51,161	51,011	150	-5
37.347701	-105.055445	495089.28	4133446.55	13RB187	556.50	3118.1	51,084	51,011	73	-82
37.347631	-105.05535	495097.69	4133438.78	13RB188	564.91	3119.1	51,154	51,011	143	-12
37.3476	-105.055255	495106.10	4133435.33	13RB189	573.32	3120.8	51,201	51,011	190	36
37.347441	-105.055135	495116.72	4133417.69	13RB190	583.94	3122	51,145	51,011	134	-21
37.347329	-105.055007	495128.05	4133405.26	13RB191	595.27	3124.4	51,126	51,011	115	-40
37.347214	-105.054932	495134.68	4133392.49	13RB192	601.90	3125.3	51,018	51,011	7	-148
37.347081	-105.054885	495138.83	4133377.74	13RB193	606.05	3126.8	51,097	51,011	86	-69
37.346946	-105.054818	495144.76	4133362.76	13RB194	611.98	3129	51,123	51,011	112	-43
37.346805	-105.054737	495151.93	4133347.11	13RB195	619.15	3130.4	51,198	51,011	187	33
37.34676	-105.054704	495154.85	4133342.12	13RB196	622.07	3131.4	51,108	51,011	97	-58
37.346613	-105.054685	495156.52	4133325.81	13RB197	623.74	3132.8	51,098	51,011	87	-68
37.346443	-105.054782	495147.92	4133306.95	13RB198	615.14	3134.2	51,049	51,011	38	-117
37.346319	-105.054779	495148.17	4133293.19	13RB199	615.39	3135	51,064	51,011	53	-102
37.346239	-105.054802	495146.13	4133284.32	13RB200		3135.9	51,062	51,011	51	-104
37.346073	-105.054885	495138.77	4133265.91	13RB201		3135.7	51,074	51,011	63	-92
37.345964	-105.0549	495137.43	4133253.82	13RB202		3137.1	51,076	51,011	65	-90
37.345827	-105.054958	495132.29	4133238.62	13RB203		3139.5	51,063	51,011	52	-103
37.345708	-105.054991	495129.36	4133225.42	13RB204		3139.5	51,055	51,011	44	-111
37.345551	-105.055032	495125.72	4133208.01	13RB205		3140	51,063	51,011	52	-103
37.3454	-105.055061	495123.14	4133191.26	13RB206		3140.7	51,043	51,011	32	-123

Latitude	Longitude	UTM easting	UTM Northing	Stations	Distance East from RB51	Altitude	Total Field Value	Base Station Value	Corrected Total Field	Anomaly
37.34525	-105.055081	495121.36	4133174.62	13RB207		3140	51,032	51,011	21	-134
37.345154	-105.055075	495121.88	4133163.97	13RB208		3141	51,028	51,011	17	-138
37.345023	-105.055071	495122.23	4133149.43	13RB209		3141.7	51,004	51,011	-7	-162
37.344862	-105.055051	495123.99	4133131.57	13RB210		3142.7	51,011	51,011	0	-155
37.344922	-105.055002	495128.33	4133138.22	13RB211		3142.7	51,018	51,011	7	-148
37.344711	-105.055046	495124.42	4133114.82	13RB212		3142.7	51,229	51,011	218	64
37.344559	-105.054993	495129.11	4133097.95	13RB213		3144.8	51,064	51,011	53	-102
37.344541	-105.055008	495127.78	4133095.96	13RB214		3143.9	51,099	51,011	88	-67
37.344368	-105.055001	495128.39	4133076.76	13RB215		3143.4	51,168	51,011	157	3
37.344256	-105.054937	495134.05	4133064.33	13RB216		3145.1	51,170	51,011	159	5
37.344118	-105.054881	495139.00	4133049.02	13RB217		3146.3	51,181	51,011	170	16
37.343952	-105.054825	495143.95	4133030.60	13RB218		3147.5	51,093	51,011	82	-73
37.34383	-105.054789	495147.13	4133017.07	13RB219		3147.2	51,081	51,011	70	-85
37.343683	-105.05475	495150.57	4133000.76	13RB220		3147.7	51,074	51,011	63	-92
37.343574	-105.054711	495154.02	4132988.66	13RB221		3147.9	51,075	51,011	64	-91
37.343441	-105.054616	495162.43	4132973.90	13RB222		3146.5	51,056	51,011	45	-110
37.343328	-105.054515	495171.37	4132961.36	13RB223		3146.7	51,099	51,011	88	-67
37.343191	-105.054393	495182.16	4132946.16	13RB224		3147	51,100	51,011	89	-66
37.343117	-105.054304	495190.04	4132937.94	13RB225		3147	51,047	51,011	36	-119
37.342957	-105.054118	495206.51	4132920.18	13RB226		3147.5	51,049	51,011	38	-117
37.342748	-105.054164	495202.42	4132897.00	13RB227		3147	51,057	51,011	46	-109

Latitude	Longitude	UTM easting	UTM Northing	Stations	Distance East from RB51	Altitude	Total Field Value	Base Station Value	Corrected Total Field	Anomaly
37.342636	-105.054313	495189.21	4132884.58	13RB228		3147.7	51,043	51,011	32	-123
37.342483	-105.054509	495171.84	4132867.62	13RB229		3147.2	51,099	51,011	88	-67
37.342364	-105.054655	495158.90	4132854.42	13RB230		3146.7	51,052	51,011	41	-114
37.342273	-105.054774	495148.36	4132844.33	13RB231		3146.3	51,070	51,011	59	-96
37.342166	-105.054881	495138.87	4132832.47	13RB232		3146.3	51,044	51,011	33	-122
37.342053	-105.054967	495131.25	4132819.94	13RB233		3146	51,057	51,011	46	-109
37.341923	-105.055109	495118.66	4132805.52	13RB234		3145.5	51,042	51,011	31	-124
37.34182	-105.055196	495110.95	4132794.10	13RB235		3145.3	51,052	51,011	41	-114
37.341687	-105.055315	495100.40	4132779.35	13RB236		3145.1	51,050	51,011	39	-116
37.341549	-105.055366	495095.87	4132764.04	13RB237		3144.1	51,041	51,011	30	-125
37.341439	-105.055482	495085.59	4132751.85	13RB238		3143.6	51,050	51,011	39	-116
37.341302	-105.055634	495072.12	4132736.65	13RB239		3143.6	51,054	51,011	43	-112
37.34123	-105.055709	495065.47	4132728.67	13RB240		3142.4	51,051	51,011	40	-115
37.341057	-105.055909	495047.74	4132709.49	13RB241		3141.5	51,036	51,011	25	-130
37.341002	-105.056071	495033.39	4132703.40	13RB242		3141.9	51,029	51,011	18	-137
37.340883	-105.056188	495023.02	4132690.20	13RB243		3141.5	51,051	51,011	40	-115
37.340793	-105.056298	495013.27	4132680.22	13RB244		3140.5	51,035	51,011	24	-131
37.34067	-105.056439	495000.77	4132666.58	13RB245		3140	51,018	51,011	7	-148
37.340528	-105.056549	494991.02	4132650.84	13RB246		3139.5	51,038	51,011	27	-128
37.340408	-105.056646	494982.42	4132637.53	13RB247		3139.3	51,028	51,011	17	-138
37.340288	-105.056726	494975.32	4132624.22	13RB248		3139	51,039	51,011	28	-127

Latitude	**Longitude**	**UTM easting**	**UTM Northing**	**Stations**	**Distance East from RB51**	**Altitude**	**Total Field Value**	**Base Station Value**	**Corrected Total Field**	**Anomaly**
37.34013	-105.056804	494968.41	4132606.69	13RB249		3138.1	51,050	51,011	39	-116
37.340015	-105.056889	494960.87	4132593.94	13RB250		3137.4	51,040	51,011	29	-126
37.339937	-105.056936	494956.70	4132585.29	13RB251		3137.8	51,038	51,011	27	-128
37.339839	-105.057152	494937.56	4132574.43	13RB252		3137.1	51,027	51,011	16	-139
37.339765	-105.057293	494925.07	4132566.23	13RB253		3136.6	51,017	51,011	6	-149
37.339698	-105.057471	494909.29	4132558.80	13RB254		3136.6	51,020	51,011	9	-146
37.339641	-105.057615	494896.54	4132552.49	13RB255		3135.9	51,029	51,011	18	-137
37.339576	-105.057768	494882.98	4132545.29	13RB256		3134.7	51,043	51,011	32	-123
37.33949	-105.057932	494868.45	4132535.75	13RB257		3133.8	51,028	51,011	17	-138
37.339495	-105.05786	494874.82	4132536.31	13RB258		3133.5	51,039	51,011	28	-127
37.339451	-105.058014	494861.18	4132531.43	13RB259		3133	51,173	51,011	162	8
37.339386	-105.058176	494846.82	4132524.23	13RB260		3133.8	51,023	51,011	12	-143
37.33933	-105.058344	494831.94	4132518.03	13RB261		3133.8	51,042	51,011	31	-124
37.33926	-105.058527	494815.73	4132510.27	13RB262		3133.3	51,041	51,011	30	-125
37.339194	-105.058686	494801.64	4132502.96	13RB263		3132.8	51,033	51,011	22	-133
37.339173	-105.058865	494785.78	4132500.64	13RB264		3131.8	51,028	51,011	17	-138
37.339085	-105.059022	494771.87	4132490.88	13RB265		3131.8	51,012	51,011	1	-154
37.339055	-105.05916	494759.64	4132487.56	13RB266		3130.9	51,035	51,011	24	-131
37.338991	-105.05937	494741.03	4132480.47	13RB267		3130.4	51,030	51,011	19	-136
37.338899	-105.059541	494725.88	4132470.28	13RB268		3129.9	51,026	51,011	15	-140
37.338815	-105.059706	494711.26	4132460.97	13RB269		3129	51,012	51,011	1	-154

Latitude	Longitude	UTM easting	UTM Northing	Stations	Distance East from RB51	Altitude	Total Field Value	Base Station Value	Corrected Total Field	Anomaly
37.338689	-105.059769	494705.67	4132446.99	13RB270		3127.5	51,019	51,011	8	-147
37.338533	-105.059765	494706.01	4132429.69	13RB271		3127	51,006	51,011	-5	-160
37.338399	-105.059693	494712.38	4132414.82	13RB272		3126.8	51,090	51,011	79	-76
37.338299	-105.059542	494725.75	4132403.71	13RB273		3127	51,053	51,011	42	-113
37.338213	-105.059429	494735.75	4132394.17	13RB274		3126.3	51,052	51,011	41	-114
37.33812	-105.059286	494748.41	4132383.84	13RB275		3125.8	51,041	51,011	30	-125
37.338041	-105.059148	494760.63	4132375.07	13RB276		3124.9	51,041	51,011	30	-125
37.337917	-105.059018	494772.14	4132361.31	13RB277		3123.9	51,042	51,011	31	-124
37.337858	-105.058917	494781.08	4132354.75	13RB278		3122.9	51,021	51,011	10	-145
37.337909	-105.058915	494781.26	4132360.41	13RB279		3122.5	51,029	51,011	18	-137
37.337827	-105.058818	494789.85	4132351.31	13RB280		3122.5	50,824	51,011	-187	-342
37.337707	-105.058691	494801.09	4132337.99	13RB281		3122.9	50,998	51,011	-13	-168
37.337616	-105.05854	494814.46	4132327.89	13RB282		3122.5	50,997	51,011	-14	-169
37.337683	-105.058584	494810.57	4132335.32	13RB283		3122	51,010	51,011	-1	-156
37.337611	-105.058483	494819.51	4132327.33	13RB284		3121.7	51,258	51,011	247	93
37.337507	-105.058356	494830.75	4132315.78	13RB285		3121.7	50,958	51,011	-53	-208
37.337395	-105.058214	494843.32	4132303.35	13RB286		3121.3	51,342	51,011	331	177
37.337308	-105.058106	494852.88	4132293.69	13RB287		3119.8	51,070	51,011	59	-96
37.337186	-105.05799	494863.15	4132280.15	13RB288		3119.1	51,024	51,011	13	-142
37.337089	-105.057863	494874.39	4132269.38	13RB289		3117.9	51,031	51,011	20	-135
37.336981	-105.057778	494881.92	4132257.40	13RB290		3116.7	51,025	51,011	14	-141

Latitude	Longitude	UTM easting	UTM Northing	Stations	Distance East from RB51	Altitude	Total Field Value	Base Station Value	Corrected Total Field	Anomaly
37.336842	-105.057674	494891.12	4132241.97	13RB291		3117.2	51,027	51,011	16	-139
37.336773	-105.057607	494897.05	4132234.31	13RB292		3116.5	51,022	51,011	11	-144
37.336593	-105.057465	494909.62	4132214.34	13RB293		3115.5	51,003	51,011	-8	-163
37.336446	-105.057375	494917.58	4132198.02	13RB294		3114.3	51,024	51,011	13	-142
37.336306	-105.057283	494925.72	4132182.49	13RB295		3113.6	50,983	51,011	-28	-183
37.33616	-105.057154	494937.14	4132166.28	13RB296		3112.6	51,021	51,011	10	-145
37.336061	-105.057054	494945.99	4132155.30	13RB297		3112.1	51,012	51,011	1	-154
37.335947	-105.056969	494953.51	4132142.64	13RB298		3111.4	51,027	51,011	16	-139
37.335793	-105.056891	494960.41	4132125.55	13RB299		3110	51,009	51,011	-2	-157
37.335661	-105.056741	494973.69	4132110.90	13RB300		3109.5	51,010	51,011	-1	-156
37.33556	-105.056688	494978.38	4132099.69	13RB301		3108.8	50,996	51,011	-15	-170
37.335399	-105.056721	494975.44	4132081.84	13RB302		3107.1	51,001	51,011	-10	-165
37.335424	-105.056736	494974.11	4132084.61	13RB303		3106.6	50,956	51,011	-55	-210
37.335377	-105.056765	494971.54	4132079.40	13RB304		3105.9	50,915	51,011	-96	-251
37.335285	-105.056824	494966.31	4132069.19	13RB305		3105.9	50,767	51,011	-244	-399
37.335225	-105.056976	494952.84	4132062.55	13RB306		3104.9	50,639	51,011	-372	-527
37.335207	-105.057101	494941.77	4132060.56	13RB307		3106.1	50,659	51,011	-352	-507
37.335226	-105.057173	494935.39	4132062.67	13RB308		3105.6	50,704	51,011	-307	-462
37.335183	-105.057251	494928.48	4132057.90	13RB309		3105.6	50,824	51,011	-187	-342
37.335179	-105.05736	494918.82	4132057.46	13RB310		3104.4	50,816	51,011	-195	-350
37.335219	-105.05744	494911.74	4132061.90	13RB311		3104.7	50,800	51,011	-211	-366

Latitude	Longitude	UTM easting	UTM Northing	Stations	Distance East from RB51	Altitude	Total Field Value	Base Station Value	Corrected Total Field	Anomaly
37.335207	-105.057532	494903.59	4132060.58	13RB312		3103.5	50,906	51,011	-105	-260
37.335258	-105.057649	494893.23	4132066.24	13RB313		3103.5	50,918	51,011	-93	-248
37.335258	-105.057722	494886.76	4132066.25	13RB314		3103.2	50,928	51,011	-83	-238
37.335225	-105.057867	494873.91	4132062.59	13RB315		3102	50,961	51,011	-50	-205
37.335209	-105.057933	494868.07	4132060.82	13RB316		3101.3	50,982	51,011	-29	-184
37.335152	-105.057984	494863.54	4132054.50	13RB317		3101.1	50,962	51,011	-49	-204
37.335094	-105.058054	494857.34	4132048.07	13RB318		3100.6	50,953	51,011	-58	-213
37.335017	-105.058127	494850.87	4132039.53	13RB319		3100.1	50,976	51,011	-35	-190
37.334937	-105.05815	494848.82	4132030.66	13RB320		3099.2	50,972	51,011	-39	-194
37.334896	-105.058217	494842.89	4132026.11	13RB321		3099.4	50,968	51,011	-43	-198
37.334856	-105.058248	494840.14	4132021.68	13RB322		3098.9	50,956	51,011	-55	-210
37.33476	-105.058273	494837.92	4132011.03	13RB323		3099.2	50,931	51,011	-80	-235
37.334664	-105.05832	494833.75	4132000.38	13RB324		3098.4	50,880	51,011	-131	-286
37.334583	-105.058331	494832.77	4131991.40	13RB325		3098.9	50,810	51,011	-201	-356
37.334604	-105.058309	494834.72	4131993.72	13RB326		3098.2	50,993	51,011	-18	-173
37.334552	-105.058351	494830.99	4131987.96	13RB327		3098.2	51,654	51,011	643	489
37.334487	-105.058375	494828.86	4131980.75	13RB328		3098.2	51,118	51,011	107	-48
37.334443	-105.058398	494826.82	4131975.87	13RB329		3097.5	51,959	51,011	948	794
37.33437	-105.058383	494828.15	4131967.77	13RB330		3097.5	51,363	51,011	352	198
37.334264	-105.05838	494828.40	4131956.01	13RB331		3097	51,129	51,011	118	-37
37.33413	-105.058399	494826.71	4131941.14	13RB332		3096.5	51,092	51,011	81	-74

Latitude	Longitude	UTM easting	UTM Northing	Stations	Distance East from RB51	Altitude	Total Field Value	Base Station Value	Corrected Total Field	Anomaly
37.33397	-105.05838	494828.38	4131923.39	13RB333		3095.5	51,093	51,011	82	-73
37.333697	-105.058297	494835.72	4131893.10	13RB334		3094.8	51,067	51,011	56	-99
37.333548	-105.058236	494841.11	4131876.57	13RB335		3093.1	51,050	51,011	39	-116
37.348845	-105.058272	494838.97	4133573.61	13RB336		3091.7	51,030	51,011	19	-136
37.348721	-105.059108	494764.92	4133559.90	13RB337		3089.8	51,033	51,011	22	-133
37.348986	-105.061615	494542.90	4133589.44	13RB351			51,017	51,017	0	-149
37.349456	-105.059889	494695.80	4133641.49	13RB352						
37.35006	-105.059052	494769.97	4133708.45	13RB353			51,005	51,017	-12	-161
37.350415	-105.05117	495468.07	4133747.42	13RB354			50,962	51,017	-55	-204
37.350709	-105.04957	495609.80	4133779.97	13RB355			50,962	51,017	-55	-204
37.350106	-105.046633	495869.88	4133712.94	13RB356			50,954	51,017	-63	-212
37.335309	-105.056842	494964.72	4132071.86	13RB357			50,968	51,017	-49	-198
37.33504	-105.058083	494854.77	4132042.08	13RB358			50,944	51,017	-73	-222
37.334618	-105.05835	494831.09	4131995.28	13RB359			50,924	51,017	-93	-242
37.327233	-105.070861	493722.19	4131176.75	13RB360			50,883	51,017	-134	-283
37.429569	-105.044877	496029.60	4142528.53	13RB361			50,878	51,017	-139	-288
37.429646	-105.044838	496033.05	4142537.07	13RB362			50,910	51,017	-107	-256
37.429735	-105.044812	496035.36	4142546.95	13RB363			50,899	51,017	-118	-267
37.429775	-105.044784	496037.83	4142551.38	13RB364			50,915	51,017	-102	-251
37.429871	-105.044735	496042.17	4142562.03	13RB365			50,856	51,017	-161	-310
				13RB366			50,852	51,017	-165	-314
				13RB367			50,928	51,017	-89	-238
				13RB368			50,892	51,017	-125	-274

Latitude	Longitude	UTM easting	UTM Northing	Stations	Distance East from RB51	Altitude	Total Field Value	Base Station Value	Corrected Total Field	Anomaly
				13RB369			50,930	51,017	-87	-236
				13RB370			50,757	51,017	-260	-409
				13RB371			50,982	51,017	-35	-184
				13RB372			50,939	51,017	-78	-227
				13RB373			50,997	51,017	-20	-169
				13RB374			50,920	51,017	-97	-246
				13RB375			50,906	51,017	-111	-260
				13RB376			50,947	51,017	-70	-219
				13RB377			51,007	51,017	-10	-159
				13RB378			50,893	51,017	-124	-273
				13RB379			50,853	51,017	-164	-313
				13RB380			50,978	51,017	-39	-188
				13RB381			50,959	51,017	-58	-207
				13RB382			51,018	51,017	1	-148
				13RB383			51,013	51,017	-4	-153
				13RB384			51,015	51,017	-2	-151
				13RB385			51,060	51,017	43	-106
				13RB386			51,031	51,017	14	-135
				13RB387			51,100	51,017	83	-66
				13RB388			51,061	51,017	44	-105
				13RB389			51,036	51,017	19	-130
				13RB390			51,025	51,017	8	-141
				13RB392						
				13RB393			50,995	51,017	-22	-171
				13RB394			50,915	51,017	-102	-251
				13RB395			51,001	51,017	-16	-165
				13RB396			50,703	51,017	-314	-463
				13RB397			51,052	51,017	35	-114
				13RB398			51,002	51,017	-15	-164
				13RB399			51,206	51,017	189	41
				13RB400			51,139	51,017	122	-27
				13RB401			51,200	51,017	183	35
				13RB402			51,143	51,017	126	-23
				13RB403			51,206	51,017	189	41
				13RB404			51,110	51,017	93	-56
				13RB405			51,164	51,017	147	-2

Latitude	Longitude	UTM easting	UTM Northing	Stations	Distance East from RB51	Altitude	Total Field Value	Base Station Value	Corrected Total Field	Anomaly
37.339969	-104.998041	500173.53	4132587.32	13RB406			51,180	51,017	163	15
37.339955	-104.998122	500166.35	4132585.77	13RB407			51,178	51,017	161	13
37.33993	-104.998117	500166.79	4132583.00	13RB408			51,179	51,017	162	14
37.339973	-104.998175	500161.66	4132587.77	13RB409			51,171	51,017	154	6
37.339983	-104.998205	500159.00	4132588.88	13RB410			51,185	51,017	168	20
37.340009	-104.998285	500151.91	4132591.76	13RB411			51,188	51,017	171	23
37.340007	-104.998338	500147.22	4132591.54	13RB412			51,183	51,017	166	18
37.340005	-104.998403	500141.46	4132591.32	13RB413			51,163	51,017	146	-3
37.340008	-104.998441	500138.09	4132591.65	13RB414			51,112	51,017	95	-54
37.34002	-104.998462	500136.23	4132592.98	13RB415			51,216	51,017	199	51
37.339997	-104.998474	500135.17	4132590.43	13RB416			51,177	51,017	160	12
37.340011	-104.998537	500129.59	4132591.98	13RB417			51,176	51,017	159	11
37.339989	-104.998609	500123.21	4132589.54	13RB418			51,055	51,017	38	-111
37.340022	-104.998674	500117.45	4132593.20	13RB419			51,164	51,017	147	-2
37.340046	-104.998711	500114.18	4132595.86	13RB420			51,120	51,017	103	-46
37.340038	-104.998758	500110.01	4132594.98	13RB421			51,133	51,017	116	-33
37.340013	-104.998811	500105.32	4132592.20	13RB422			51,160	51,017	143	-6
37.340032	-104.998819	500104.61	4132594.31	13RB423			51,177	51,017	160	12
37.340028	-104.998909	500096.64	4132593.87	13RB424			51,194	51,017	177	29
37.340023	-104.998939	500093.98	4132593.31	13RB425			51,214	51,017	197	49

Latitude	Longitude	UTM easting	UTM Northing	Stations	Distance East from RB51	Altitude	Total Field Value	Base Station Value	Corrected Total Field	Anomaly
37.340031	-104.999009	500087.78	4132594.20	13RB427			51,198	51,017	181	33
37.34004	-104.999071	500082.29	4132595.20	13RB428			51,201	51,017	184	36
37.340056	-104.999114	500078.48	4132596.97	13RB429			51,188	51,017	171	23
37.340088	-104.999218	500069.27	4132600.52	13RB430			51,192	51,017	175	27
				13RB431			51,198	51,017	181	33
				13RB432			51,105	51,017	88	-61

APPENDIX D

ACTUAL GRAVITY MODELS

A-A' GRAVITY MODEL

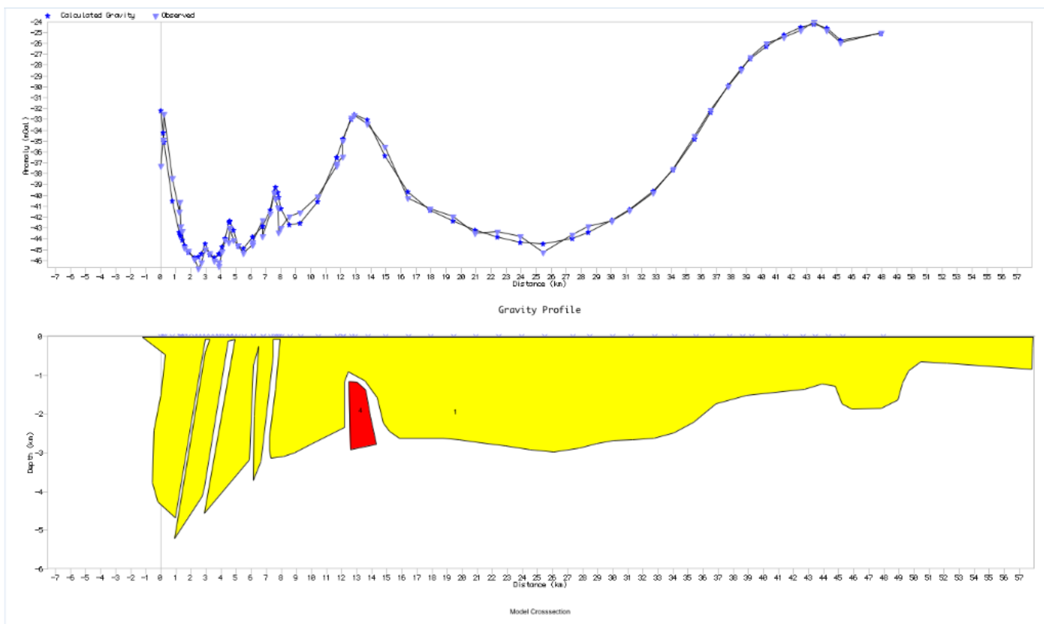

B-B' GRAVITY MODEL

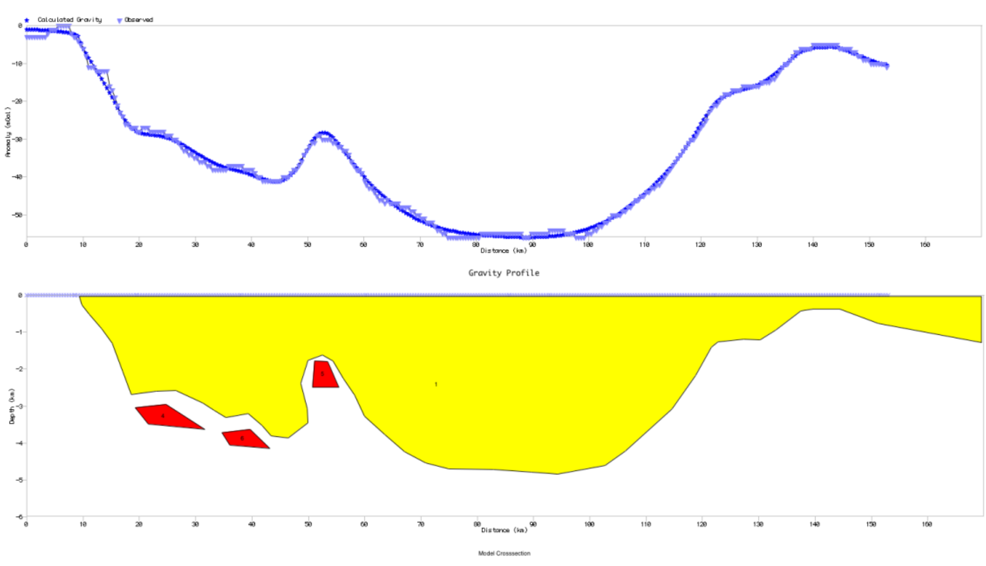

APPENDIX E

GRAVMAG GRAVITY MODELS SAVE FILES

A-A' GRAVITY CROSS-SECTION

LeftEdge,-7508.189

RightEdge,58022.83

Bottom,6000

ProfileAzimuth,0

Latitude,36

Body,1,-0.4,0.001,71,0.0001,0,0.9680399

X,-1213.963,Z,-17.48852

X,57921.31,Z,-17.48852

X,57870.55,Z,-293.9082

X,57819.79,Z,-846.7475

X,52185.44,Z,-688.7934

X,50459.61,Z,-649.3049

X,49647.45,Z,-886.2361

X,49241.37,Z,-1202.144

X,48936.81,Z,-1636.518

X,47820.09,Z,-1853.705

X,45891.22,Z,-1873.449

X,45231.34,Z,-1735.239

X,44774.5,Z,-1281.121

X,43911.58,Z,-1221.889

X,42744.1,Z,-1360.098

X,38886.35,Z,-1510.757

X,36880.45,Z,-1730.336

X,35383.92,Z,-2209.102

X,34064.16,Z,-2494.774

X,32744.4,Z,-2623.731

X,31323.13,Z,-2663.22

X,30054.13,Z,-2682.964

X,28937.41,Z,-2761.941

X,27769.94,Z,-2880.407

X,26094.86,Z,-2987.449

X,24521.3,Z,-2919.895

X,22896.99,Z,-2821.174

X,21272.67,Z,-2742.197

X,19800.63,Z,-2663.22

X,18734.67,Z,-2623.731

X,17364.16,Z,-2623.731

X,15841.36,Z,-2623.731

X,15181.48,Z,-2446.033

X,14775.4,Z,-2228.846

X,14369.32,Z,-1577.285

X,13557.17,Z,-1142.911

X,12440.45,Z,-905.9803

X,12186.65,Z,-1182.4

X,12186.65,Z,-2347.311

X,10054.73,Z,-2761.941

X,8887.256,Z,-2998.872

X,8125.857,Z,-3097.593

X,7313.699,Z,-3137.082

X,7212.179,Z,-2919.895

X,7212.179,Z,-2603.987

X,7618.258,Z,-1360.098

X,7922.818,Z,-76.72131

X,7465.979,Z,-76.72131

X,7465.979,Z,-511.0951

X,6653.821,Z,-3216.059

X,6146.222,Z,-3709.666

X,6196.982,Z,-2051.148

X,6501.541,Z,-247.718

X,6146.222,Z,-748.0262

X,5892.422,Z,-3176.57

X,2897.589,Z,-4558.669

X,4927.984,Z,-76.72131

X,4471.145,Z,-116.2098

X,2897.589,Z,-3885.344

X,2745.309,Z,-4124.295

X,917.9529,Z,-5210.23

X,2948.349,Z,-412.3738

X,3252.908,Z,-76.72131

X,2948.349,Z,-76.72131

X,968.7128,Z,-4677.134

X,-198.7647,Z,-4253.188

X,-554.084,Z,-3770.23

X,-464.6369,Z,-2428.527

X,4.274836,Z,-1513.98

X,308.8342,Z,-477.9475

X,-554.084,Z,-224.6951

Color,255,255,0

Body,4,0.1,0.001,6,0.0001,0,0.9680399

X,12491.21,Z,-1162.656

X,13049.57,Z,-1182.4

X,13607.93,Z,-1379.843

X,13912.48,Z,-2052.517

X,14318.56,Z,-2784.423

X,12592.73,Z,-2921.092

Color,255,0,0

B-B' GRAVITY CROSS-SECTION

LeftEdge,0

RightEdge,170000

Bottom,6000

ProfileAzimuth,0

Latitude,36

Body,1,-0.3,0.001,47,0.0001,0,0.9680399

X,9334.248,Z,-35.60831

X,169581.7,Z,-37.87104

X,169581.7,Z,-1282.018

X,151214.8,Z,-765.5786

X,144330.8,Z,-373.8872

X,139663.7,Z,-373.8872

X,137446.8,Z,-427.2997

X,133013,Z,-943.6202

X,130212.8,Z,-1210.682

X,127295.8,Z,-1192.878

X,122745.4,Z,-1264.095

X,121578.6,Z,-1406.528

X,118720,Z,-2172.107

X,114577.9,Z,-3080.119

X,106293.8,Z,-4219.585

X,102656.9,Z,-4613.122

X,94291.25,Z,-4833.858

X,89550.74,Z,-4793.724

X,82858.25,Z,-4713.456

X,74910.92,Z,-4693.389

X,70867.54,Z,-4532.854

X,67103.02,Z,-4231.851

X,63617.35,Z,-3770.313

X,59992.25,Z,-3268.64

X,58179.71,Z,-2706.767

X,56227.73,Z,-2265.296

X,54415.18,Z,-1783.69

X,52540.67,Z,-1623.155

X,49953.52,Z,-1763.624

X,48698.68,Z,-2385.697

X,49814.1,Z,-3088.038

X,49953.52,Z,-3449.242

X,46467.85,Z,-3870.647

X,43400.46,Z,-3810.446

X,41770.76,Z,-3525.223

X,39320.52,Z,-3204.748

X,35313.71,Z,-3308.774

X,33253.26,Z,-3115.727

X,31269.73,Z,-2919.881

X,26485.93,Z,-2581.602

X,22985.59,Z,-2599.407

X,18551.82,Z,-2688.427

X,17035,Z,-2065.282

X,15168.15,Z,-1299.703

X,13284.28,Z,-900.7473

X,11084.42,Z,-516.3205

X,9800.961,Z,-267.0623

Color,255,255,0

Body,4,0.2,0.001,4,0.0001,0,0.9680399

X,19251.89,Z,-3044.51

X,24735.76,Z,-2955.49

X,31619.77,Z,-3632.047

X,21585.45,Z,-3489.614

Color,255,0,0

Body,5,0.1,0.001,4,0.0001,0,0.9680399

X,51068.94,Z,-1785.953

X,53439.19,Z,-1806.02

X,55391.17,Z,-2488.294

X,50790.09,Z,-2488.294

Color,255,0,0

Body,6,0.1,0.001,4,0.0001,0,0.9680399

X,34653.4,Z,-3721.068

X,39670.56,Z,-3632.047

X,43170.9,Z,-4148.368

X,36053.53,Z,-4059.347

Color,255,0,0

REFERENCES

AMEC Environment & Infrastructure, INC., 2012, Freeman 3-24 Well Nontributary determination Huerfano County, Colorado Raton Basin, AMEC Project Number: DE1016003A.

Baltz, E. H., 1965, Stratigraphy and history of Raton Basin and notes on San Luis basin, Colorado-New Mexico: Am. Assoc. Petroleum Geologists Bull., v. 49, p. 2041-2075.

Close, J.C., Dutcher, R.R., 1990, Update on Coalbed methane potential, Raton Basin, Colorado and New Mexico. In Proceedings: 1990 SPE Annual Technical Conference and Exhibition.

Cooper, J.R., 2006, Igneous Intrusions and Thermal Evolution in the Raton Basin, CO-NM: Contact Metamorphism and Coal Bed Methane Generation, University of Missouri-Columbia, Masters Dissertation, p. 5-10.

Flores, R.M.,1987, Sedimentology of Upper Cretaceous and Tertiary siliciclastics and coals in the Raton Basin, New Mexico and Colorado: New Mexico Geological Society Guidebook, 38th Field Conference, Northeastern New Mexico, p. 255-264.

Flores, R.M., Bader, L. R., 1999, A summary of Tertiary coal resources of the Raton Basin, Colorado and New Mexico. In USGS Professional Paper 1625-A.

Hemborg, H. T., 1998, Spanish Peak Field, Las Animas County, Colorado: Geologic setting and early development of a coalbed methane reservoir in the Central Raton Basin. Colorado Geological Survey, Dept. of Natural Resources, Denver, CO, Resource Series 33, 34 p.

Highley, D.K., 2007, Petroleum Systems and Assessment of Undiscovered Oil and Gas in the Raton Basin–Sierra Grande Uplift Province, Colorado and New Mexico, U.S. Geological Survey, Reston, Virginia, U.S. Geological Survey Digital Data Series DDS–69–N, p. 3-33.

Hildenbrand, T.G., Briesacher, A., Flanagan, G., Hinze, W.J., Hittelman, A.M., Keller, G.R., Kucks, R.P., Plouff, D., Roest, W., Seeley, J., Smith, D.A., and Webring, M., 2002, Rationale and Operational Plan to Upgrade the U.S. Gravity Database: U.S. Geological Survey OpenFile Report 02–463, 12 p.

Hinze, W.J., 2003, Bouguer reduction density, why 2.67?: Geophysics, v. 68, p. 1559–1560, doi: 10.1190/1.1620629.

Hoffman, G.K., and Brister B.S., 2003, New Mexico's Raton Basin coalbed methane play, New Mexico Bureau of Geology and Mineral Resources Bulletin, Volume 25, Number 4.

Holom, D.I., and Oldow, J.S., 2007, Gravity reduction spreadsheet to calculate the Bouguer anomaly using standardizedmethods and constants, Geosphere: v.3; no.2; p.86-90.

Johnson, R.B., 1961, Coal resources of the Trinidad coal field in Huerfano and Las Animas counties, Colorado, B 1112-E, p. 129-180, illus., tables, geol. Map.

Johnson, R.B., 1986, Geology of the igneous rocks of the Spanish Peaks region Colorado. Geological Survey Professional Paper 594-G.

Johnson, R.C., and Finn, T.M., 2001, Potential for a Basin-Centered Gas Accumulation in the Raton Basin, Colorado and New Mexico, U.S. Geological Survey Bulletin 2184-B, p. 5-9.

Lee, P.M., 2005, Spatial, temporal and petrogenic relationships of basaltic and lamprophyric dikes and sills of the Raton Basin, southern Colorado and northern New Mexico. University of Missouri-Columbia, Masters Thesis, 160 p.

Lindsey D.A., 2010, The Geologic Story of Colorado's Sangre de Cristo Range, U.S Geologic Survey Circular 1349.

Mariita, N.O., 2007, The Magnetic Method, Presented on short course II on surface exploration fo geolthermal resources.

Miggins, D.P., 2002, Chronological, Geochemical and Isotopic Framework of Igneous Rocks within the Raton Basin and Adjacent Rio Grande Rift, South- Central Colorado and Northern New Mexico. University of Colorado, Boulder, Masters Thesis.

Penn, B.S., 1995, An investigation of the temporal and geochemical characteristics, and the petrogenetic origins of the Spanish Peaks intrusive rocks of south-central Colorado: Co. School of Mines, Ph.D. Thesis

Pillmore, C. L., 1969, Geology and coal deposits of the Raton coal field, Colfax Co., New Mexico: The Mountain Geologist, v. 6, p. 125-142.

Pillmore, C.L., and Flores, R.M., 1987, Stratigraphy and depositional environments of the Cretaceous-Tertiary boundary clay and associated rocks, Raton Basin, New Mexico and Colorado, *in* Fassett, J.E., and Rigby, J.K., Jr., eds., The Cretaceous-Tertiary Boundary in the San Juan and Raton Basins: New Mexico and Colorado: Geological Society of America, Special Paper 209, p. 111-130.

Speer, W.R., 1976, Oil and Gas Exploration in the Raton Basin, New Mexico Geol. Soc. Guidebook, 27th Field Conf., Vermejo Park, 1976, p. 217-226.

Stevens, S.H., Lombardi, T.E., Kelso, B.S., and Coates, J.M., 1992, A geologic assessment of natural gas from coal seams in the Raton and Vermejo Formations, Raton Basin. GRI Topical Report 92/0345.

Tremain, C.M., 1980, The Coal Bed Methane Potential of the Raton Mesa Coal Region, Raton Basin, Colorado. Colorado Geological Survey Open-File Report 80-4.

Tweto,O., 1975, Laramide (Late Cretaceous–early Tertiary) orogeny in the southern Rocky Mountains, in Curtis, B., ed., Cenozoic Geology of the Southern Rocky Mountains: Geologic Society of America Memoir 144, p. 1–44.

Tweto, O., 1979, Geologic map of Colorado: US. Geological Survey in corporation with the Colorado Geological Survey, scale 1:500,000.

Woodward, L.A., 1976, Structural framework of the southern Raton Basin New Mexico, New Mexico Geologic Society Guidebook, 27^{th} Field Conference.

Woodward, L.A., 1987, Tectonic framework of northeastern New Mexico and adjacent parts of Colorado, Oklahoma and Texas. New Mexico Geological Society Guidebook, 38th Field Conference.

BIOGRAPHICAL SKETCH

Yusuf Pehlivan was born on the 11th of November, 1986, in Istanbul, Turkey. He received his Bachelor of Science degree in Geological Engineering from the Dumlupinar University in the spring of 2010. After graduation, he was awarded full financial support by Turkish Petroleum Corporation for graduate study in the USA. Then, he enrolled in a graduate program at the Florida State University, Department of Earth, Ocean, and Atmospheric Sciences in the fall of 2012. His major is Structural Geology. Yusuf's thesis, Gravity, Magnetic, and Geologic Constraints on the Raton Basin of Southern Colorado, is supervised by Dr. David W. Farris. Yusuf Pehlivan has presented his research as a poster presentation at the Geological Society of America 125th anniversary annual meeting in Denver, Colorado in October, 2013. After completing his Master's degree in Spring'15 semester, he will be employed as an expert geologist by the Turkish Petroleum Corporation.